

1 Multi-Site Non-Methane Hydrocarbon Source Apportionment and Ozone Insights  
2 in Southern Taiwan Using Positive Matrix Factorization

3 Duy-Hieu Nguyen<sup>1</sup>, Hsin-Cheng Hsieh<sup>1</sup>, Mao-Chang Liang<sup>2</sup>, Neng-Huei Lin<sup>3</sup>, Chieh-Heng Wang<sup>4\*\*</sup>, Jia-Lin Wang<sup>1\*</sup>

4 <sup>1</sup> Department of Chemistry, National Central University, Taoyuan, 320317, Taiwan

5 <sup>2</sup> Institute of Earth Sciences, Academia Sinica, Taipei 115201, Taiwan

6 <sup>3</sup> Department of Atmospheric Science, National Central University, Taoyuan, 320317, Taiwan

7 <sup>4</sup> Center for Environmental Studies, National Central University, Taoyuan, 320317, Taiwan

8 *Correspondence to:*

9 \*Jia-Lin Wang ([cwang@cc.ncu.edu.tw](mailto:cwang@cc.ncu.edu.tw))

10 \*\* Chieh-Heng Wang ([chwang1110@gmail.com](mailto:chwang1110@gmail.com))

11 **Abstract**

12 Ozone pollution remains a persistent challenge in Taiwan's Kaoping region due to dense industrial and  
13 urban emissions. Using high-resolution, hourly observations from three Photochemical Assessment  
14 Monitoring Stations (PAMS) combined with Positive Matrix Factorization (PMF), this study resolved  
15 eight distinct sources of non-methane hydrocarbons (NMHCs), key precursors of ozone formation. The  
16 time-resolved PMF output captured source-specific temporal patterns—as shown by the acetylene factor  
17 at Linyuan ( $R^2 = 0.99$  with observations)—providing an intrinsic check on model performance and  
18 facilitating spatial interpretation of sources. Petroleum-related emissions dominate NMHC mass at all  
19 sites but are more prominent at Xiaogang, while aged air masses substantially enhance ozone pollution  
20 at downwind locations such as Linyuan and Chaozhou, underscoring the role of regional transport and  
21 atmospheric aging. Although mixed sources from vehicular and solvent emissions contributed less mass,  
22 they dominated ozone formation potential (OFP) due to higher chemical reactivity. Notably, their  
23 influence persisted even under moderate ozone conditions, indicative of a VOC-limited regime. Overall,  
24 these results emphasize that effective ozone mitigation in southern Taiwan requires coordinated control  
25 of petroleum, mobile, and solvent emissions, and demonstrate the value of multi-site, year-round, high-  
26 time-resolution NMHC measurements for constraining ozone precursors.

27 **1 Introduction**

28 Volatile organic compounds (VOCs) are key precursors in atmospheric chemistry and play a  
29 substantial role in determining air quality (Guan et al., 2020; Guo et al., 2017; Finlayson-Pitts and Pitts  
30 Jr, 1993). In the presence of nitrogen oxides (NO<sub>x</sub>) and sunlight, VOCs undergo photochemical reactions  
31 that lead to the formation of ground-level ozone (O<sub>3</sub>), while their oxidation products contribute to  
32 secondary organic aerosol formation (Wu et al., 2024; Mcfiggans et al., 2019). These processes are  
33 particularly intensified in rapidly industrializing and urbanizing regions, where elevated emissions and  
34 complex atmospheric interactions amplify air pollution (Zhang et al., 2022). The resulting decline in air  
35 quality poses substantial risks to both human health and ecosystems (Ramírez et al., 2019; Xu et al.,  
36 2022). Given their complex roles and diverse emission sources, a detailed characterization of ambient  
37 VOCs is essential to advance our understanding of their source origins, chemical behavior, and  
38 contributions to air pollution.

39 The impact of VOCs on ozone formation critically depends on the local chemical regime—whether  
40 ozone production is VOC-limited or NO<sub>x</sub>-limited (Kleinman et al., 2002; Sillman, 1999). In VOC-limited  
41 environments, common in densely industrialized and urbanized areas, ozone levels are more responsive  
42 to changes in reactive VOC concentrations, whereas in NO<sub>x</sub>-limited conditions, ozone formation is  
43 constrained by nitrogen oxide availability. Several studies in East and Southeast Asia have emphasized  
44 this spatial heterogeneity of ozone sensitivity (Li et al., 2019; Wang et al., 2021; Ren and Xie, 2022). In  
45 Taiwan, both modeling and observational evidence indicate that southern and western regions typically  
46 exhibit VOC-limited or transition regimes, while rural and downwind areas are more NO<sub>x</sub>-limited (Chang  
47 et al., 2022; Chen et al., 2021b). This regime dependence underscores the need for region-specific  
48 precursor management and highlights the importance of identifying the dominant reactive VOC sources  
49 that most effectively drive ozone formation. Understanding these sensitivities provides an essential  
50 framework for interpreting ozone formation potential (OFP) derived from NMHC source contributions.

51 Traditional VOC source analysis often relies on passive sampling techniques, such as using  
52 canisters at strategic locations to capture spatial and temporal variations in ambient concentrations  
53 (Dumanoglu et al., 2014; Mo et al., 2015; Wang et al., 2018; Dong et al., 2024). While effective for  
54 regional assessments, these methods lack the high temporal resolution required for detailed source  
55 apportionment. To overcome this limitation, automated gas chromatograph (auto-GC) systems have been  
56 developed, offering continuous, high-frequency VOC measurements that better support the analysis of  
57 dynamic emission patterns (Wernis et al., 2022; Su et al., 2016; Chen et al., 2014; Henry, 2013). In  
58 Taiwan, the Environmental Protection Administration (EPA) has established a Photochemical  
59 Assessment Monitoring Stations (PAMS) network to provide real-time NMHCs monitoring data—a  
60 subset of VOCs—forming a technical foundation for evidence-based air quality management and  
61 research. These sophisticated monitoring techniques form a foundation for detailed source apportionment  
62 studies (Chen et al., 2021a; Gu et al., 2020; Languille et al., 2020), enabling more accurate evaluation of  
63 emission contributions and their temporal variations. Initially, this network lacked a standardized  
64 approach for identifying specific NMHC sources, with only one of the nine stations incorporating  
65 targeted source-tracking capabilities in 2007 (Chen et al., 2014). However, since 2013, the network has  
66 expanded to track emissions from major industrial zones, growing to a total of 15 stations to better  
67 support the EPA's regulatory and scientific objectives (Nguyen et al., 2025).

68 The Kaoping region, located in southern Taiwan, is home to one of the country's largest industrial  
69 complexes, situated near Kaohsiung Port—an important maritime trade hub in East Asia (Yeh et al.,  
70 2022). This region faces persistent air quality challenges due to intensive industrial activity, including  
71 petrochemical manufacturing, steel production, and power generation, which collectively represent  
72 dominant sources of anthropogenic NMHC emissions (Huang and Hsieh, 2019). In addition to the  
73 industrial activities, multiple emission sources—including vehicular traffic, ships in ports, urban  
74 development, biogenic activity, and long-range transport of pollutants further burden the area's air quality  
75 (Chou et al., 2022; Lin et al., 2007). Vehicular emissions, particularly those associated with gasoline  
76 combustion and fuel evaporation, are recognized as significant contributors to ambient NMHC levels in

77 urbanized environments. These sources are commonly characterized by elevated concentrations of light  
78 alkanes and related gasoline-associated species (Shao et al., 2016; Mo et al., 2017). At the same time, the  
79 presence of isoprene from vegetation and meteorological processes—such as sea-land breeze circulations  
80 and seasonal monsoons—complicates the chemical transformation and transport of NMHCs across the  
81 region (Li and Wang, 2012; Cheng et al., 2016). The local EPA authority has implemented emission  
82 control strategies targeting major industrial zones to address these environmental concerns. These  
83 measures include stricter emission standards, technical support for pollution reduction, and mandatory  
84 installation of factory gas recovery and treatment systems. Despite these efforts, residents adjacent to  
85 industrial parks continue to express concerns about air quality issues (Ko, 1996; Deng et al., 2022),  
86 suggesting that current measures have not fully mitigated the impact of VOC emissions on surrounding  
87 communities. Given these complex and intertwined emission sources, high-resolution NMHC  
88 monitoring from the PAMS network in the Kaoping region offers a valuable database for investigating  
89 source contributions and understanding their influence on regional air quality to improve air pollution  
90 management and air quality.

91 To quantitatively determine the contribution of different emission sources, receptor models such  
92 as Chemical Mass Balance (CMB) and PMF are widely applied in atmospheric research (Su et al., 2019;  
93 Na and Kim, 2007; Liu et al., 2008b; Lingwall and Christensen, 2007). Each approach has its strengths  
94 and limitations. CMB requires detailed and well-characterized source profiles and is sensitive to  
95 collinearity among input species, which can limit its applicability in complex source environments. In  
96 contrast, PMF is a data-driven technique that extracts source profiles and their contributions directly from  
97 ambient measurements, making it more flexible in situations where comprehensive source profiles are  
98 unavailable but depend on a sufficiently large and high-quality dataset (Su et al., 2016). Recent advances  
99 allow PMF to incorporate auxiliary information (e.g., known marker species or source profiles),  
100 improving source identification accuracy (Yang et al., 2022). In this context, the continuous, speciated  
101 NMHC data provided by the PAMS network create an ideal foundation for applying PMF to source  
102 apportionment in the Kaoping region, where emission sources are diverse. However, identifying sources  
103 is only one part of the broader picture of air quality. To fully understand pollution dynamics in this region,  
104 it is also essential to consider meteorological factors that influence the dispersion, accumulation, and  
105 transport of NMHCs.

106 To address this, many studies have coupled PMF with the Conditional Probability Function (CPF),  
107 which integrates PMF-resolved source contributions with wind direction data to infer the likely directions  
108 of pollution sources (Pekney et al., 2006; Zhou et al., 2018; Pallavi and Sinha, 2019). CPF analyses  
109 typically rely on the time series of factor contributions generated by PMF to calculate conditional  
110 probabilities of wind directions associated with elevated contributions (e.g., using the 75th percentile  
111 threshold). While CPF enhances the spatial interpretation of PMF outputs, it primarily focuses on wind  
112 direction patterns and does not fully exploit the rich temporal variability captured in the PMF-resolved  
113 factor time series. Consequently, these temporal features are rarely used to further investigate source  
114 behavior, even though they contain valuable information, such as peak events, seasonal trends, or

115 episodic spikes in individual sources. Importantly, high-contribution events in specific time windows  
116 provide an opportunity to integrate PMF with air mass back-trajectory analysis, linking these peaks to  
117 possible upwind source regions. This approach enhances the interpretability of PMF beyond statistical  
118 association and opens new avenues for spatiotemporal source identification.

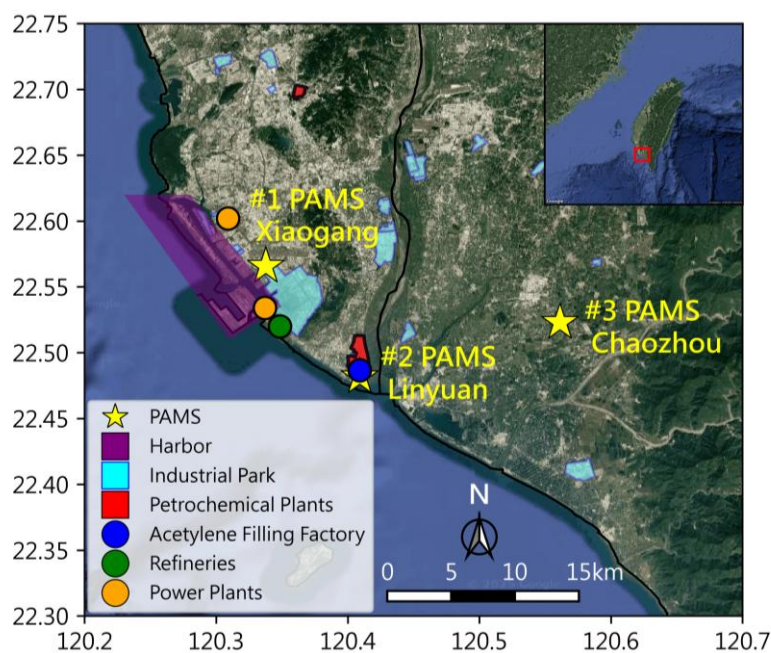
119 In Taiwan, PMF has been widely applied to support evidence-based air-quality policymaking;  
120 however, most studies have concentrated on northern (Kuo et al., 2014; Liao et al., 2017; Liao et al.,  
121 2024) and central regions (Su et al., 2019). Applications of CPF in conjunction with PMF have also been  
122 largely limited to central Taiwan (Huang and Hsieh, 2019; Chen et al., 2019), leaving the Kaoping region  
123 comparatively understudied—particularly in terms of combining PMF, CPF, and trajectory analyses to  
124 identify industrial and transported NMHC sources. Thus, this study aims to bridge this gap by applying  
125 PMF and CPF to identify and characterize NMHC sources in the Kaoping region and analyze the  
126 temporal features of PMF factor contributions to guide trajectory-based source tracking. By identifying  
127 high-contribution episodes for source factor and performing back-trajectory analyses during those  
128 episodes, we can confidently infer the likely geographic origins of the emissions. In addition, the OFP  
129 associated with each source was estimated to evaluate its relative impact on ozone production. Compared  
130 to most PMF studies that rely on data from a single receptor site and limited time resolution, our study  
131 leverages three PAMS sites with year-round hourly data and distinct source–receptor characteristics,  
132 allowing for a more robust source apportionment and regional representation. This multi-PAMS  
133 framework offers insights into NMHC dynamic emissions and transport in one of the most industrialized  
134 areas in Southern Taiwan.

## 135 **2 Methodology**

### 136 **2.1 Study site description**

137 This study focuses on source apportionment of ambient NMHCs in the highly industrialized  
138 Kaoping region of southern Taiwan, approximately one-third the size of the New York metropolitan  
139 region, based on measurements from three PAMS monitoring sites: Xiaogang, Linyuan, and Chaozhou.  
140 The distinct locations of three sites and environmental settings provide a comprehensive view of source–  
141 receptor relationships across the region. Xiaogang, located in southern Kaohsiung, is a mixed urban–  
142 industrial area heavily influenced by emissions from multiple industrial activities. These include large  
143 petrochemical complexes, a regional airport, steel mills, metallurgical processing plants, shipyards, and  
144 power stations. In addition, maritime operations from Kaohsiung Harbor—one of the busiest ports in  
145 Asia—contribute significantly to local NMHC levels. Linyuan, situated along the southwestern coast and  
146 downwind of Kaohsiung’s industrial corridor, is situated next to a large petrochemical complex  
147 frequently receiving high-concentration plumes from nearby facilities under the influence of coastal  
148 meteorology. Chaozhou, by contrast, is more inland and characterized by agricultural and vegetative land  
149 use, with minimal influence from industrial and urban anthropogenic sources. However, due to its  
150 geographic position downwind of the Kaohsiung industrial corridor, Chaozhou is susceptible to the  
151 regional pollution transported from neighboring urban and industrialized areas. As such, it serves as a  
152 receptor site for background air quality conditions with intermittent influence from upwind

153 anthropogenic emissions. Together, the three sites offer spatial and environmental contrasts that support  
154 robust source apportionment and allow for evaluation of both local emission characteristics and regional  
155 transport dynamics in the Kaoping region.



156  
157 **Figure 1:** Study region with marked industrial facilities. Base map from Google Maps (Map data ©2025  
158 Google)

## 159 2.2 Data collection

160 All three sites are equipped with PAMS, enabling high-temporal-resolution measurements of  
161 speciated NMHCs (Fig. S1). Each station employs an automated gas chromatograph system (Clarus 500  
162 GC, PerkinElmer), configured with dual flame ionization detectors (FIDs) and thermal desorption units  
163 (TM-TD1, PerkinElmer). This TD-GC/FID setup allows for hourly quantification of 54 NMHC species  
164 ranging from C<sub>2</sub>–C<sub>11</sub>. Ambient air is sampled at a flow rate of 15 mL/min over 40 minutes, yielding  
165 approximately 600 mL of air per sample, and then passes through a Nafion dryer (500 sccm counter-flow)  
166 to eliminate excess humidity during sample collection. No ozone scrubber is needed, as the system  
167 features short, inert-coated sampling tubing, effectively minimizing the likelihood of ozone reactions.  
168 Samples are pre-concentrated at –30 °C and desorbed at 325 °C for GC injection. A two-column  
169 separation strategy with a Deans switch is implemented to improve chromatographic resolution.  
170 Following desorption, analytes are first transferred to the BP-1 column. The Deans switch is then routes  
171 lighter hydrocarbons (C<sub>2</sub>–C<sub>5</sub>) from the BP1 column to an Al<sub>2</sub>O<sub>3</sub> PLOT column (50 m × 0.32 mm i.d.,  
172 5.0 μm, Varian), while heavier compounds (C<sub>6</sub>–C<sub>11</sub>) are directed through an uncoated column. Instrument  
173 calibration is conducted every three days using certified standard gas mixtures containing the 54 target  
174 species (Spectra Gases, Branchburg, USA), ensuring data quality with a measurement precision (1σ)  
175 maintained below 4%.

176 In addition to VOC measurements, this study incorporates hourly ancillary data from the Taiwan  
177 Air Quality Monitoring Network (TAQMN), including O<sub>3</sub> and meteorological parameters such as wind

178 speed and wind direction. This integrated dataset supports a comprehensive analysis of photochemical  
179 activity, emission dynamics, and pollutant transport mechanisms across the three monitoring  
180 environments: urban-industrial-port (Xiaogang), coastal-industrial (Linyuan), and inland-rural  
181 (Chaozhou). Data cleaning was performed prior to analysis to ensure consistency across datasets.  
182 TAQMN measurements were first screened to remove invalid entries, including missing values,  
183 instrument flags, any non-numeric values associated with routine maintenance, calibration events, power  
184 outages, or temporary instrument shutdowns. After this quality-control procedure, the TAQMN 2024  
185 dataset achieves approximately 98% data coverage across the three sites.

### 186 2.3 NMHC source apportionment model

187 PMF is a receptor-based modeling technique widely used for identifying and quantifying  
188 contributions of pollution sources to ambient air quality. Originally developed by Paatero and Tapper  
189 (1994) and refined in subsequent work (Paatero, 1997), PMF has been extensively applied to NMHCs  
190 source apportionment in various urban and industrial environments (Guo et al., 2011; Zhang et al., 2015).  
191 The method decomposes the observed concentration matrix ( $X$ ) into two non-negative matrices: the  
192 source contribution matrix ( $G$ ) and the source profile matrix ( $F$ ), along with a residual matrix ( $E$ ). The  
193 model accounts for measurement uncertainty and identifies latent factors representing individual sources,  
194 each characterized by a distinct chemical profile and temporal pattern. Detailed mathematical  
195 formulations are described in prior studies (Su et al., 2019; Han et al., 2023; Huang and Hsieh, 2019).

196 In this study, we applied the U.S. EPA's PMF 5.0 software to perform source apportionment of  
197 NMHCs measured at the three PAMS sites in the Kaoping region. The input to the model consisted of  
198 concentration and uncertainty matrices constructed from hourly NMHC measurements. Uncertainty ( $U_{ij}$ )  
199 was calculated based on species concentrations ( $X_{ij}$ ) and minimum detection limits (MDL) as follows:

$$200 U_{ij} = \sqrt{(0.5 \times MDL_j)^2 + (error\ fraction \times X_{ij})^2} \quad (1)$$

201 For concentrations below MDL, the value was substituted with half MDL with uncertainty set at  $\frac{5}{6}$   
202 MDL, and an error fraction (10%). Missing values were excluded from the input dataset to maintain  
203 model reliability. To ensure a consistent and robust dataset across the three sites and four seasons, species  
204 selection was based on signal-to-noise (S/N) ratios and detection frequency following EPA PMF  
205 guidance. Specifically, species with S/N ratios  $< 0.1$  or missing data with occurrences more than 4  
206 instances were classified as "bad" and excluded, while those with  $0.1 \leq S/N < 2$  were down-weighted as  
207 weak species. This screening process resulted in a final set of 22 out of the 54 species that were  
208 consistently detectable and quantitatively reliable across all sites and seasons (Table S1). Model stability  
209 was then evaluated through multiple diagnostic procedures. First, factor numbers from 3 to 8 were tested,  
210 each with 100 independent runs using random seed initialization. The optimal number of factors was  
211 selected based on  $Q_{(robust)}/Q_{(true)}$  values that were close to 1.0, reproducibility of factor profiles across runs  
212 assessed via Bootstrap (BS) analyses ( $>95\%$  matching), and the interpretability and physical plausibility  
213 of the resulting source profiles. Together, these procedures confirm that the PMF solution provides a  
214 robust and well-constrained representation of NMHC sources in the study region, while the consistent  
215 selection of 22 species ensures comparability across all seasonal and site-specific analyses.

## 216 2.4 Directional analysis with CPF and trajectory modeling

217 The CPF was employed to identify the likely directional origins of pollution sources by analyzing  
218 the relationship between elevated PMF factor timeseries contributions and wind direction. First, source  
219 contribution timeseries obtained from PMF output were used, with each factor representing a distinct  
220 emission source (e.g., petrochemical, solvent usage, aged air mass). Wind speed and wind direction data  
221 were integrated with PMF output to determine directional influence.

$$222 \text{CPF}_{\Delta\theta} = n_{\Delta\theta}/m_{\Delta\theta} \quad (2)$$

223 CPF was computed as the ratio of the number of times the factor contributions exceeded the  
224 threshold within a given wind sector ( $n_{\Delta\theta}$ ) to the total number of valid observations in that sector ( $m_{\Delta\theta}$ ).  
225 Wind direction was divided into 16 equal intervals ( $22.5^\circ$  per sector) to ensure robust analysis. For each  
226 PMF-resolved factor, the 70<sup>th</sup> percentile was the threshold to isolate the plume events, as it effectively  
227 filtered out moderate events while retaining sufficient data for statistically stable and interpretable CPF  
228 results (Table S2). Higher CPF values in specific wind sectors indicated stronger contributions from  
229 sources in that direction. CPF plots were generated for each PMF factor to visualize dominant source  
230 directions and assess consistency with known emission source locations, meteorological patterns, and  
231 local topography.

232 Our developed trigger back-trajectory is employed to further utilize the time series features from  
233 PMF factor contribution, particularly their episodic spikes or peak events. Unlike traditional Lagrangian  
234 models such as HYSPLIT, which simulate long-range air mass transport using synoptic meteorological  
235 fields, the trigger back-trajectory model is optimized for short-range, near-surface pollution episodes  
236 using high-resolution wind observations from receptor sites. Each trajectory is then visualized and  
237 mapped using GIS tools layered onto spatial imagery via the Google Maps API. By aggregating multiple  
238 trajectories associated with similar high-concentration events, a trajectory ensemble analysis is  
239 conducted to identify convergence zones, which are likely source regions. This hybrid approach improves  
240 the spatial interpretability of PMF results by complementing factor profiles and CPF with spatiotemporal  
241 back-tracing, providing a robust framework for identifying not just what the sources are, but when and  
242 where they likely originated.

## 243 2.5 Ozone formation potential and uncertainty consideration

244 The OFP of each NMHC species was estimated using the Maximum Incremental Reactivity (MIR)  
245 coefficients developed by (Carter, 2010). The OFP for compound  $i$  was calculated as:

$$246 \text{OFP}_i = C_i \times \text{MIR}_i \quad (3)$$

247 Where  $C_i$  (ppb) is the measured mixing ratio of the species, and  $\text{MIR}_i$  ( $\text{g O}_3 \text{ g}^{-1} \text{ VOC}$ ) is its  
248 reactivity coefficient (Table S1). The MIR scale represents ozone yield under low VOC/ $\text{NO}_x$  (i.e., high-  
249  $\text{NO}_x$  or VOC-limited) conditions, where ozone formation is primarily sensitive to changes in VOC  
250 abundance. This assumption aligns with previous photochemical studies indicating that ozone formation  
251 in southern Taiwan is predominantly VOC-limited (Chang et al., 2022).

252 The uncertainty associated with OFP estimation was inherently accounted for during the PMF  
253 analysis. These uncertainties were used to construct the PMF input uncertainty matrix, which determines  
254 the weighting of each data point in the model fitting. As the OFP was calculated from the PMF-resolved

255 factor contribution time series, the measurement uncertainties are inherently reflected in the factor  
256 contributions. While this approach propagates measurement uncertainty into OFP estimates, it is  
257 important to note that OFP represents a photochemical potential, not realized ozone formation, and does  
258 not capture the nonlinear interactions that govern actual ozone production.

### 259 **3 Results and discussion**

#### 260 **3.1 PAMS data overview**

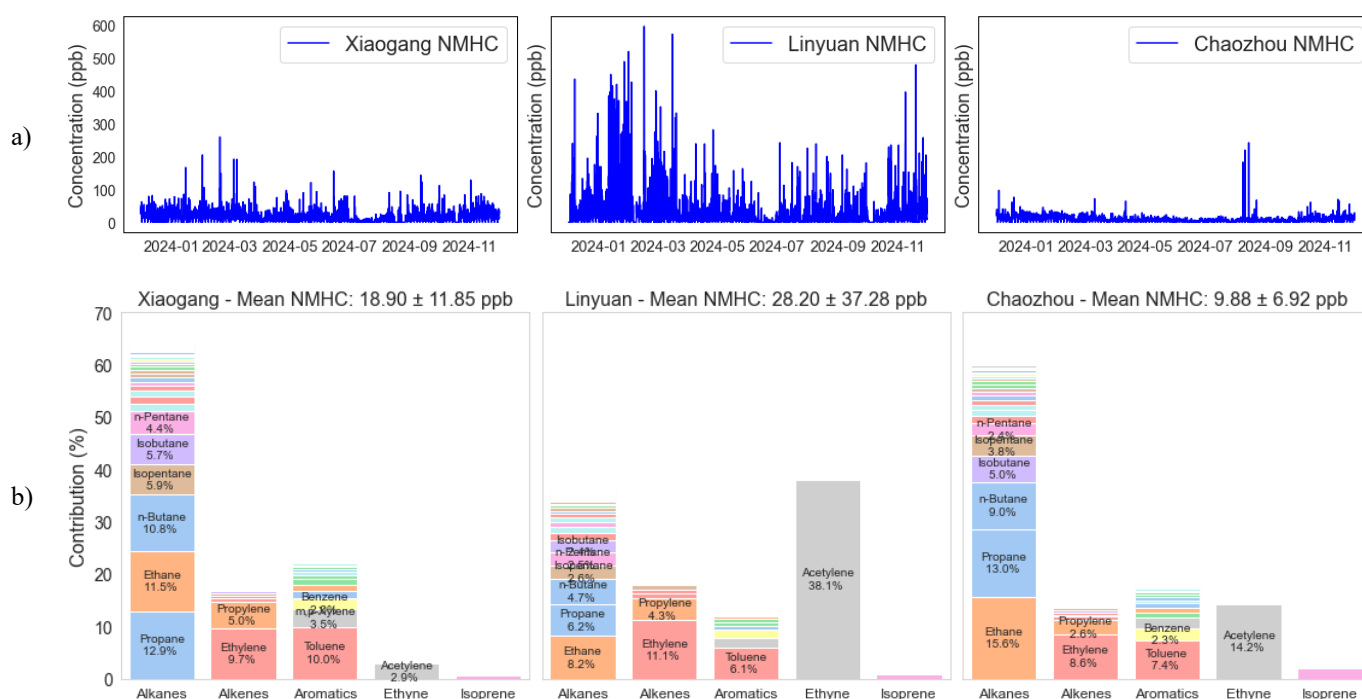
261 Leveraging three PAMS sites in a region with heavy industrial loading, this study captures the  
262 spatial variability of source dynamics, providing a clearer picture of how NMHC levels are shaped. The  
263 annual mean concentrations of NMHC—calculated from 54 species—exhibited pronounced spatial  
264 heterogeneity across the sampling sites. As illustrated in Fig. 2a, the level varied considerably, with  
265 Linyuan recording the highest average concentration ( $28.20 \pm 37.28$  ppb), followed by Xiaogang ( $18.90$   
266  $\pm 11.85$  ppb) and Chaozhou ( $9.88 \pm 6.92$  ppb). However, the corresponding median values (10.92, 13.68,  
267 and 6.92 ppb, respectively) indicate that these distributions are skewed, particularly at Linyuan, where  
268 the mean is substantially higher than the median, reflecting occasional extreme emission events likely  
269 driven by dense petrochemical operations. Meanwhile, Xiaogang, with a mean slightly higher than its  
270 median, represents a mixed urban-industrial setting, where both vehicular emissions and industrial  
271 activities contribute to ambient NMHC levels. In contrast, Chaozhou exhibits lower mean and median  
272 concentrations, characteristic of a predominantly agricultural environment. Notably, an anomalous  
273 elevation was observed in Chaozhou during August, and this feature will be further examined in later  
274 sections. Statistical analysis reveals that, after removing the elevated window, the extreme short-duration  
275 did not alter the central tendency of the observations, with minimal impact observed on the statistical  
276 metrics (Table S3). A comparative analysis indicates that NMHC concentrations in this study were  
277 generally lower than those reported in Guangzhou (42.74 ppb), Wuhan (34.65 ppb), Chengdu (41.8 ppb),  
278 and Beijing (29.12 ppb), which were selected due to their similar urban environments (Li et al., 2022;  
279 Hui et al., 2018; Zou et al., 2015; Song et al., 2018). The difference reflects the effectiveness of emission  
280 control measures in Taiwan, supported by stringent regulations, cleaner fuels, and strengthened industrial  
281 emission standards (Moe, 2022, 2023). Additionally, meteorological factors, such as higher wind speeds  
282 at Xiaogang and Chaozhou, likely contribute to dilution and dispersion, further shaping the observed  
283 NMHC distribution. The combined consideration of mean and median reveals both typical ambient levels  
284 and the influence of short-term emission peaks in understanding NMHC exposure across the region.

#### 285 **3.2 NMHC compositions**

286 While NMHC concentrations provide a broad picture of emission intensities, a more detailed  
287 understanding of their pollution requires an analysis of their chemical composition. The NMHC profiles  
288 at Chaozhou, Linyuan, and Xiaogang exhibited distinct characteristics, reflecting their diverse emission  
289 sources and atmospheric processing (Fig. 2b). Across all sites, 54 NMHC species were quantified and  
290 categorized into five major groups: alkanes, alkenes, aromatics, alkynes (ethyne), and isoprene.

291 Alkanes dominated the NMHC composition at Chaozhou and Xiaogang, comprising 61% and 64%  
292 of total NMHC, respectively, while accounting for only 36% at Linyuan. This alkane dominance is

293 consistent with previous findings in Asian cities (Zhang et al., 2020; Song et al., 2020), reflecting their  
 294 long atmospheric lifetimes and broad emission sources, including hydrocarbon processing and gasoline-  
 295 related activities. Ethane, propane, n-butane, and isobutane alone contributed about 42% of the total  
 296 concentration across three sites, with enhanced levels of n-butane and isobutane particularly evident at  
 297 Xiaogang and Chaozhou. In contrast, Linyuan exhibited a distinctly different chemical profile, with  
 298 ethyne (acetylene) making up 38% of its total NMHCs, substantially higher than at Chaozhou (14%) and  
 299 Xiaogang (3%). This substantial presence of acetylene indicates localized, intense anthropogenic  
 300 activities. Notably, Linyuan recorded the highest annual mean NMHCs. However, this ranking is  
 301 primarily driven by its elevated acetylene levels. When acetylene is excluded, the relative ranking  
 302 changes, and Linyuan shifts to second place after Xiaogang (Fig. S2), highlighting the disproportionate  
 303 influence of a single pollutant species on the site's total NMHC burden.



304 **Figure 2:** Time series of total NMHC concentrations and mean composition of NMHC groups at  
 305 Chaozhou, Linyuan, and Xiaogang in 2024. (a) Hourly variations illustrate temporal patterns and notable  
 306 episodic peaks at each site. (b) Mean NMHC concentrations (ppb) and percentage contributions of  
 307 individual compounds within major chemical groups. The mean concentrations of individual species are  
 308 presented in Fig. S3.

309 Aromatic compounds formed the second-largest group at Xiaogang (22%), followed by Chaozhou  
 310 (17%) and Linyuan (13%). The predominance of toluene and m,p-xylene across all sites aligns with  
 311 findings from previous studies in Shanghai (Zhang et al., 2018) and Xi'an (Song et al., 2020), indicating  
 312 contributions from solvent use, paint application, and industrial processes. The notably higher toluene  
 313 proportion at Xiaogang suggests significant emissions from solvent-related industries, such as coating  
 314 and painting. Alkenes accounted for a relatively stable fraction across sites (approximately 14% at  
 315 Chaozhou, 18% at Linyuan and Xiaogang), with ethylene being the dominant species. Given that  
 316 ethylene is primarily emitted from combustion and petrochemical activities, its consistent presence  
 317 underscores the role of anthropogenic sources in shaping the NMHC composition.

318 These pronounced differences in NMHC chemical profiles highlight the spatial heterogeneity of  
319 emission sources and atmospheric processes across the study area. The alkane-rich profiles of Chaozhou  
320 and Xiaogang contrast sharply with the ethyne-dominated composition at Linyuan, illustrating how  
321 industrial activities significantly influence ambient NMHC signatures. Understanding these chemical  
322 distinctions is crucial for designing targeted pollution control strategies tailored to the unique emission  
323 characteristics of each urban environment.

### 324 3.3 Resolved Source profiles

325 As mentioned before, some measured NMHCs were excluded from PMF analysis due to their  
326 greater volume of data below MDLs. Consequently, the numbers of NMHC species input into the model  
327 for source apportionment were 22 species, accounting for 88.9%, 91.7%, and 93.8% of the full 54  
328 NMHCs concentration at Xiaogang, Linyuan, and Chaozhou, respectively. Based on the model used,  
329 there were eight distinct sources of resolved factors (Figs. 3, 5, and S4) which are petrochemical I (Petro  
330 I), petrochemical II (Petro II), refinery, industrial fugitive emissions, mixed sources (Mixed),  
331 photochemical aged (Aged air mass), acetylene, and biogenic. Consistent source profiles were observed  
332 across seasons and at all three monitoring sites, underscoring the robustness of the PMF results and  
333 confirming the dominant contribution of specific source factors throughout the study area (Fig. 3).

#### 334 3.3.1 Common sources

##### 335 a) Petrochemical factors

336 The PMF analysis revealed a strong presence of ethylene and propylene, both of which are key raw  
337 materials in the petrochemical industry (Leuchner and Rappenglück, 2010). Ethylene is the most  
338 important feedstock in the synthetic organic chemical manufacturing industry, serving as a building block  
339 for a wide array of chemicals for making plastics, antifreeze solutions, and solvents. Similarly, propylene  
340 is a critical precursor in producing various petrochemical products. Our results are in agreement with  
341 those of Xie and Berkowitz (2006), who reported that ethylene and propylene were the main NMHCs  
342 emitted from petrochemical emissions. The factor represented by a single dominant compound of  
343 ethylene and propylene can be referred to here as the Petro-I and II (Fig. 3). Ethylene and propylene did  
344 not appear in proportion despite their shared industrial origin due to the spatial heterogeneity in emission  
345 sources across the large campus of the petro-complex at the studied sites. Notably, in summer, the Petro-I  
346 profile becomes especially pronounced at Xiaogang, characterized by increased ethane and propane as  
347 by-products of cracking operations (Thiruvenkataswamy et al., 2016; Pedrozo et al., 2020). They are  
348 prone to fugitive emissions or evaporative losses, particularly from storage tanks at elevated temperatures.

349 The PMF-resolved time series contribution for Petro-I and Petro-II reveals episodic spikes, with  
350 no clear pattern of increase or decrease during weekends (Fig. S5), suggesting these events may be  
351 associated with perennial petrochemical processes with constant fugitive emissions. Linyuan consistently  
352 exhibits the highest contributions for both Petro-I and II during winter and, to a lesser extent, spring and  
353 fall, followed by a distinct decline in summer. In contrast, Xiaogang's Petro-I contributions rise notably  
354 in fall and remain elevated into the winter with a lesser extent in spring, though Petro-II activity there is  
355 less pronounced. Chaozhou records consistently low contributions for both factors throughout all seasons,

356 indicating minimal influence from these industrial sources (Fig. S5, green line). Spatial analysis of the  
357 preferred source directions for Petro-I and II further underscores site-specific differences. At Xiaogang,  
358 the dominant influence comes from northerly winds in fall, spring, and winter (Fig. 4, red line), while  
359 stronger southerly winds are observed in summer and peak in fall, emphasizing the role of prevailing  
360 winds in the Kaohsiung area. It highlights the complexity of source contributions and the importance of  
361 meteorological conditions in modulating observed concentrations. This pattern aligns with the spatial  
362 distribution of active petrochemical facilities in Kaohsiung City, as shown in Fig. 1, and is reflected in  
363 the dominant source directions in Fig. 4. For Linyuan, the prevailing source direction is from the  
364 northwest, consistent with the site location downwind of Linyuan industrial areas (Fig. 4, orange line).

#### 365 *b) Refinery factor*

366 The refinery-related emissions were primarily composed of C3–C5 alkanes, including propane,  
367 isobutane, n-butane, isopentane, and n-pentane (Fig. 3). While n-pentane is commonly identified as a  
368 tracer of gasoline evaporation in VOC source profiles, and n-butane is also abundant in fuel vapors  
369 (Kumar et al., 2020), they are also associated with emissions from petroleum refining processes (Wei et  
370 al., 2016). The separation of refinery and petrochemical sources in PMF analyses has also been  
371 documented in previous studies (Kim et al., 2005; Buzcu and Fraser, 2006; Dumanoglu et al., 2014; Chen  
372 et al., 2019) and in CMB modeling (Scheff et al., 1989). The PMF-resolved time series contributions are  
373 relatively stable and exhibit consistent patterns across most sites and seasons, except for a notable  
374 increase at Xiaogang during summer (Fig. S5). Occasional peaks in the PMF-resolved time series at  
375 Xiaogang and Linyuan suggest the presence of episodic events or localized influences, likely associated  
376 with butanes, which are the most dominant contributors to this factor. Yet, there is no clear indication of  
377 a long-term trend or significant weekend effect, highlighting the ongoing and process-driven nature of  
378 refinery emissions. Chaozhou consistently registers the lowest refinery factor contributions in all seasons,  
379 likely due to its inland downwind position and limited proximity to major refinery facilities. Directional  
380 analysis reveals that the preferred source direction for this factor is southeast (SE) for Xiaogang and  
381 northwest (NW) for Linyuan, reflecting the locations of refinery facilities relative to each monitoring site  
382 (Fig. 4).

#### 383 *c) Industrial fugitive emissions*

384 Isopentane and n-pentane are recognized tracers of natural gas operations (Gilman et al., 2013) or  
385 gasoline vapor emissions (Gentner et al., 2009). In our PMF results, both species showed elevated  
386 concentrations, indicating a strong contribution from fugitive sources (Fig. 3). Because isopentane and  
387 n-pentane exhibit similarly OH reaction rates (Atkinson, 1986), their ratio ( $iC_5/nC_5$ ) is commonly used  
388 to identify emission sources (Bourtsoukidis et al., 2019). Accordingly, we examined this ratio across all  
389 sites using the PMF-resolved concentration of species from factor profile output to reveal their distinct  
390 relationship between isopentane and n-pentane.

391 Many studies report that an  $iC_5/nC_5$  ratio in the range of approximately 0.8–1.1 is characteristic of  
392 oil & natural gas operations or raw-gas emissions (Gilman et al., 2013; Thompson et al., 2014; Swarhout  
393 et al., 2013; Gilman et al., 2010). In our analysis, the  $iC_5/nC_5$  ratio was consistently  $<1$  across the sites

394 and seasons, with site-specific seasonally mean values of  $0.53 \pm 0.02$  at Linyuan,  $0.76 \pm 0.06$  at Xiaogang,  
395 and  $0.87 \pm 0.10$  at Chaozhou, all within or below the typical oil & natural gas range. The Kaoping region  
396 hosts only downstream industrial activities—such as refining, petrochemical processing, and feedstock  
397 production—rather than upstream extraction. Therefore, this factor was attributed to industrial fugitive  
398 emissions, likely originating from petrochemical processing units, storage tanks, and refinery-related  
399 leakage. The lowest ratio at Linyuan reflects a very local, fresh fugitive leak from proximate  
400 refinery/petrochemical sources. In contrast, the downwind receptor (Chaozhou) or the mixed urban-  
401 industrial area (Xiaogang) can result in higher ratios.

402 The PMF-resolved time series of industrial fugitive emission at all three sites—Xiaogang, Linyuan,  
403 and Chaozhou—exhibit a stable, low-level temporal pattern characteristic of continuous industrial  
404 fugitive emission sources across all seasons (Fig. S5). Occasional minor peaks occurred, with slightly  
405 higher values at Xiaogang and Linyuan than at Chaozhou at times, but no major episodic events were  
406 observed. This pattern underscores the nature of fugitive pollution, which remains a minor and relatively  
407 steady contributor to ambient NMHC levels year-round.

408 CPF analysis further reveals distinct spatial and seasonal patterns. At Linyuan and Xiaogang,  
409 elevated CPF values are associated with winds from the N-NW, and SE-SSE sectors, respectively,  
410 suggesting that elevated concentrations are most likely to occur under these prevailing wind conditions  
411 (Fig. 4). Winter and spring generally show slightly higher CPF values compared with summer and fall,  
412 particularly at these industrial sites, reflecting seasonal variations in atmospheric transport or emission  
413 dynamics.

414 In contrast, Chaozhou consistently displays low CPF values and the lowest NMHCs abundance  
415 across all seasons and wind directions, reflecting its rural setting, lack of industrial activity, and its  
416 downwind position relative to Xiaogang and Linyuan. The combination of weaker PMF-resolved  
417 timeseries (Fig. S5) and nearly uniform ratios of pentane isomers ( $0.87 \pm 0.10$ ) indicates that fugitive  
418 emissions reaching Chaozhou are largely diluted and regionally transported rather than locally generated.  
419 The winter enhancement is also consistent with the compositionally altered profile observed at Chaozhou  
420 (Fig. S4a), where atmospheric processing during transport and seasonal stagnation modifies the alkane  
421 distribution while retaining the broader characteristics of industrial fugitive emissions. Overall, the  
422 temporal and directional indicators confirm that Chaozhou is primarily influenced by diluted, downwind  
423 industrial fugitive emissions, with local contributions becoming detectable only under wintertime  
424 stagnation.

#### 425 *d) Mixed factor*

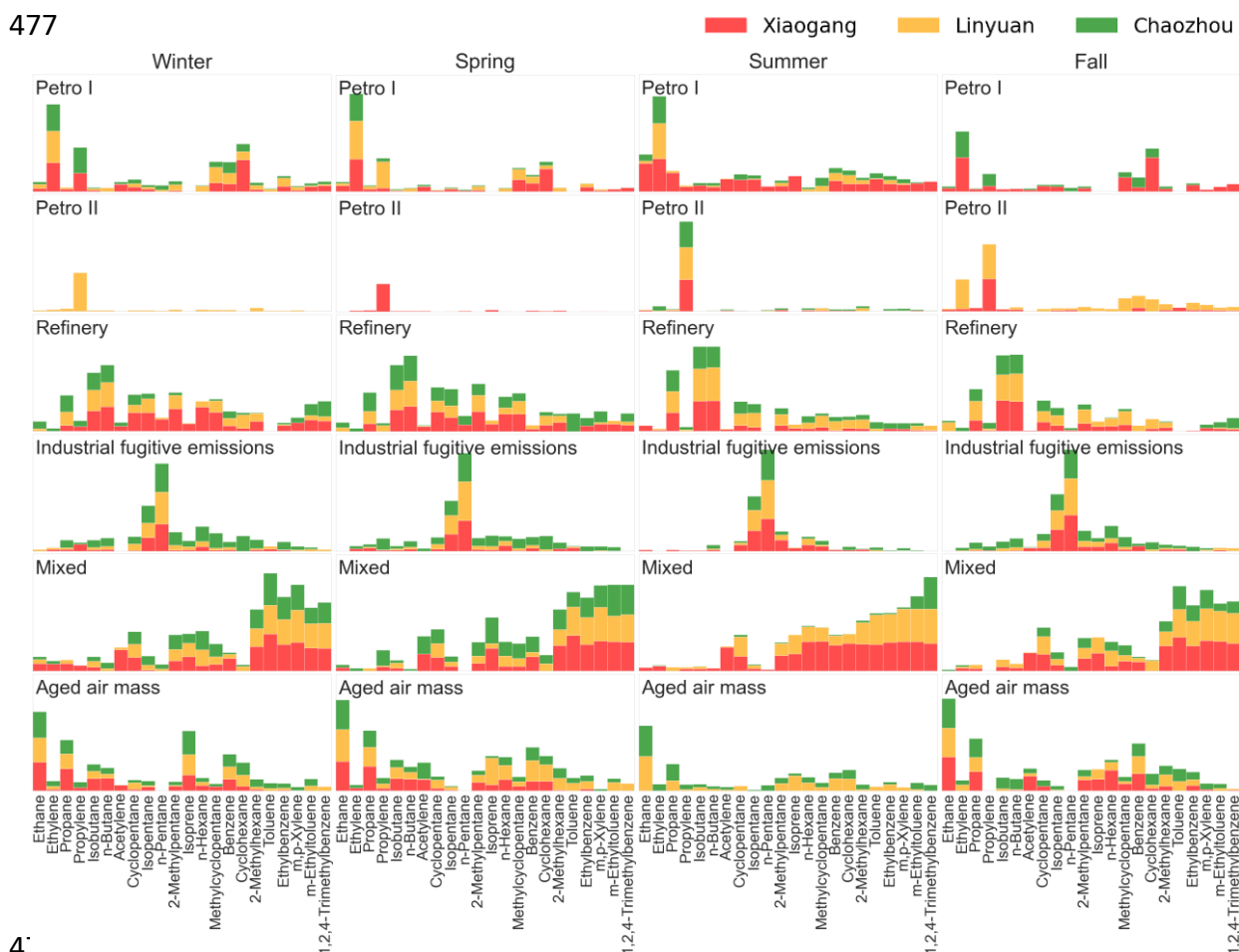
426 In this study, distinguishing between vehicular and solvent-related emissions proved challenging,  
427 primarily because Kaohsiung City hosts large-scale petrochemical complexes, shipyards, and harbor  
428 facilities. Our PMF analysis was unable to resolve these sources as distinct factors but instead  
429 appropriately captured this complexity under a single, mixed source factor (Fig. 3). This likely reflects  
430 the complex emission environment of the region and possibly the proximity in distance of these source  
431 types, where vehicular activities and solvent usage co-occur, contributing overlapping NMHC species

432 such as toluene, benzene, ethylbenzene, etc (Chang et al., 2003). A major limitation in separating these  
433 sources is the absence of key tracers, such as 2,2,4-trimethylpentane (Huang and Hsieh, 2019), 2,3-  
434 dimethylbutane as recognized tracer of motor vehicle exhaust (Chang et al., 2004), or such as methyl  
435 tert-butyl ether (MTBE), as an indicator for vehicle exhaust or evaporation (Rubin et al., 2006; Chang  
436 et al., 2003; Lin et al., 2005), which makes it challenging to fully separate and resolve vehicle emissions.  
437 Another limitation is that CO, a commonly used tracer of combustion sources (Huang and Hsieh, 2019),  
438 was considered in the test PMF runs; however, its diagnostic value was restricted in the Kaoping region  
439 because multiple overlapping CO sources (e.g., traffic, industrial, residential burning, etc.) all  
440 contributed to elevated CO levels. As a result, the PMF model grouped vehicles and solvent-related  
441 emissions into a single mixed factor, reflecting the complex emission environment and overlapping  
442 NMHC signatures.

443 As a result, the mixed source factor exhibits contributions from both vehicular emissions and  
444 solvent-related industrial activities. Cai et al. (2010) reported that ethylene and propylene are major  
445 products of internal combustion engines, and both were present in our mixed factor. Additionally,  
446 acetylene—a known tracer of incomplete combustion—along with toluene, benzene, and m,p-xylene,  
447 typify vehicular emissions, further supporting the presence of traffic-related contributions (Nelson and  
448 Quigley, 1984; Baker et al., 2008; Liu et al., 2008a; Xu et al., 2017). Cyclopentane, 2-methylpentane,  
449 and methylocyclopentane are primarily markers of evaporation or unburned fuel from vehicles, rather  
450 than direct combustion products. Isoprene may also be present in vehicle exhaust, especially under  
451 conditions of incomplete combustion (e.g., cold starts, older engines, or engines lacking effective  
452 emission controls) (Nakashima et al., 2010; Park et al., 2011; Zou et al., 2019) or from tire wear (Jung  
453 and Choi, 2023). Moreover, the elevated contribution of heavier aromatic compounds (Fig. 3) suggests  
454 a further influence from diesel truck exhaust (Wang et al., 2024). The frequent presence of heavy-duty  
455 diesel trucks transporting steel, chemicals, machinery, and other goods was a common sight on the roads  
456 of Xiaogang and Linyuan, serving as the logistical backbone for multiple heavy industries in the region.  
457 Importantly, toluene is the dominant compound in the mixed factor, especially in Xiaogang, which  
458 provides a key constraint on source interpretation. The elevated toluene contribution points primarily to  
459 substantial solvent usage, as toluene is widely employed in paints, adhesives, coatings, and various  
460 cleaning agents, and chemical manufacturing processes common in industrial zones, along with  
461 ethylbenzene, m,p-xylene, n-hexane, and 1,2,4-trimethylbenzene (Wu et al., 2016; Shen et al., 2018;  
462 Shao et al., 2016). Together, the combined presence of combustion tracers, evaporative fuel markers,  
463 and solvent-related aromatics demonstrates that this factor represents a true mixture of vehicular exhaust  
464 and industrial solvent usage, with toluene-dominated solvent emissions (Bari and Kindzierski, 2018),  
465 serving as a major driver of its chemical profile. This mixed source factor highlights gaps in current  
466 emission inventories and underscores the need for improved, locally speciation-resolved data to support  
467 future research in this region.

468 By observing PMF-resolved time series (Fig. S5), the mixed factor exhibits strong seasonality,  
469 with its contributions peaking in winter, reaching the lowest levels in spring and summer, and rising

470 again in the fall. Xiaogang and Linyuan consistently display higher values than Chaozhou, especially  
 471 during peak winter and late fall, highlighting the greater influence of industrial and traffic activities near  
 472 these sites. While generally lower and more consistent, Chaozhou still shows some variability,  
 473 indicating a minor but persistent influence from mixed sources. Interestingly, the mixed source factor  
 474 often demonstrates a weekly concentration pattern characterized by elevated weekday levels and lower  
 475 concentrations on weekends (Baidar et al., 2015; Pollack et al., 2012), further supporting the  
 476 contribution from traffic-related emissions.



479 **Figure 3:** Summary of common source profiles of NMHC at the three sites in 2024. This figure presents  
 480 the percentage contribution of six common source factors (Petro I, Petro II, Refinery, Industrial fugitive  
 481 emissions, Mixed, and Aged air mass) to the total NMHC burden at three monitoring sites: Xiaogang  
 482 (red), Linyuan (orange), and Chaozhou (green) across four seasons (Winter, Spring, Summer, and Fall).  
 483 Each panel represents a specific source factor and season combination. The stacked bars within each panel  
 484 show the relative contribution of NMHC species to that source factor. Consistent source profiles of  
 485 fingerprint species were observed across seasons and at all three monitoring sites, underscoring the  
 486 robustness of the PMF results.

487 Across all seasons, CPF values for the mixed factor remain relatively stable and uniform,  
 488 suggesting that the contributing sources are predominantly local and affected by winds from multiple  
 489 directions. However, during the fall, there is a noticeable increase in CPF values from the NW and NNW

490 sectors, corresponding with the onset and intensification of the northeastern monsoon (Fig. 4). This shift  
491 results in more frequent and stronger winds from these directions, enabling enhanced transport from  
492 upwind or regional sources and producing more pronounced CPF values from NW and NNW. Meanwhile,  
493 the elevated time series contributions observed during winter are likely due to accumulation in the  
494 atmosphere, driven by a lower mixing layer height, which promotes the buildup of locally emitted  
495 pollutants (Fig. S5).

496 *e) Aged air mass factor*

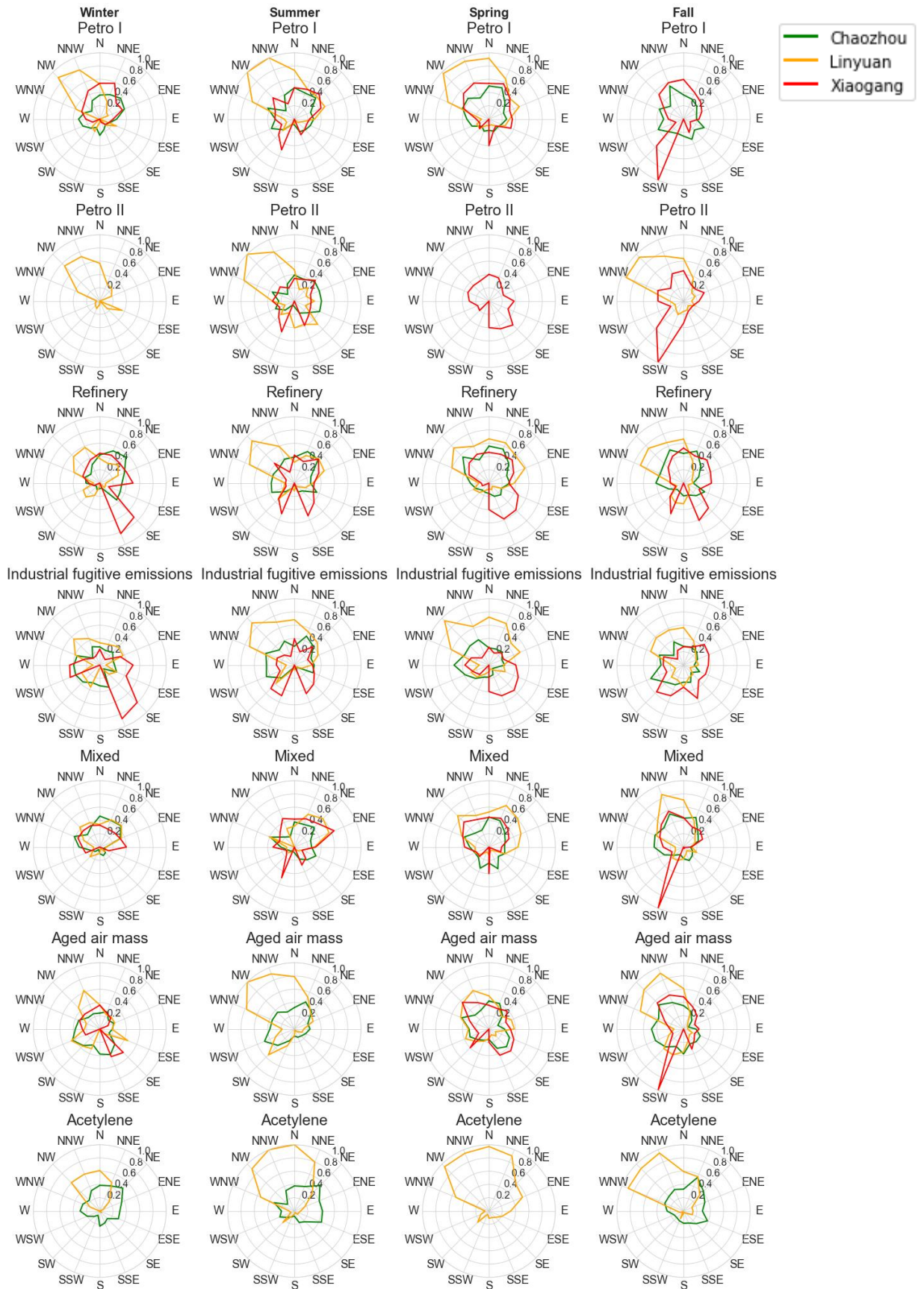
497 The aged air mass factor was characterized by a dominant presence of low-reactivity, long-lived  
498 (NMHCs), including ethane, propane, acetylene, and benzene (Fig. 3). These compounds are  
499 sufficiently stable to survive long-range atmospheric transport due to their relatively slow reaction rates  
500 with hydroxyl (OH) radicals. The atmospheric chemical lifetimes of these VOCs range from several  
501 days to months, allowing them to persist in the environment and become enriched over time (Atkinson  
502 and Arey, 2003; Lau et al., 2010). Such compositional features suggest that the aged air mass is primarily  
503 influenced by secondary and transported sources rather than recent local emissions. Ethane, in particular,  
504 often dominates this factor due to its long atmospheric lifetime, and its strong presence aligns with  
505 findings from previous studies (Chen et al., 2010; Li et al., 2015). Similarly, benzene and acetylene are  
506 frequently observed in aged air masses, consistent with the findings of Wu et al. (2016), suggesting  
507 regional transport rather than local fugitive emissions as their primary source.

508 The PMF-resolved time series of the aged air mass factor reveals distinct seasonal trends.  
509 Contributions from aged air mass rise in late fall, peaking during winter, most notably at Xiaogang and  
510 Linyuan (Fig. S5, the red and orange lines). This elevated influence persists into spring before gradually  
511 declining, a pattern that closely mirrors the strengthening and subsequent weakening of the northern  
512 monsoon. While Chaozhou is located further inland, its aged air mass time series remains comparable  
513 to those at Xiaogang and Linyuan, though slightly lower in magnitude. This suggests that Chaozhou is  
514 still significantly influenced by long-range transport and potentially nearby sources from the vicinity  
515 areas. These spatial differences underscore the critical role of seasonal wind direction and site location  
516 in shaping the transport and accumulation of aged air masses across the sites.

517 Analysis of CPF values further supports these findings, with generally higher values observed  
518 from the NW to N wind sectors (Fig. 4), consistent with the prevailing northern monsoon during late  
519 fall through spring. Xiaogang and Linyuan display pronounced CPF peaks in these directions,  
520 reinforcing their susceptibility to long-range transport and downwind positioning during the monsoon.  
521 This pattern aligns well with the elevated time series signals observed at these sites during winter and  
522 early spring.

523 By contrast, Chaozhou exhibits lower CPF values and less direct influence from the northern  
524 monsoon. Instead, the CPF values at Chaozhou are enhanced under western wind conditions, suggesting  
525 that local factors, such as inland positioning and the influence of sea–land breeze circulation, modulate  
526 its exposure to aged air mass transported from Xiaogang and Linyuan. Fig. S6 further supports this  
527 observation as it shows the wind profile during day & night in alignment with the sea-land breeze pattern

528 at Kaohsiung. Taken together, these patterns highlight the interplay of regional transport, seasonal  
529 meteorology, and site-specific geography in determining the concentration and source influence of aged  
530 air masses across the study area. In summary, the six common factors—Petro I, Petro II, refinery,  
531 industrial fugitive emissions, mixed, and aged air mass—represent the dominant anthropogenic and  
532 transported NMHC sources across the Kaoping region.



533 **Figure 4:** CPF results viewing the direction for the highest 30% of factor contribution

### 534 3.3.2 Distinct sources

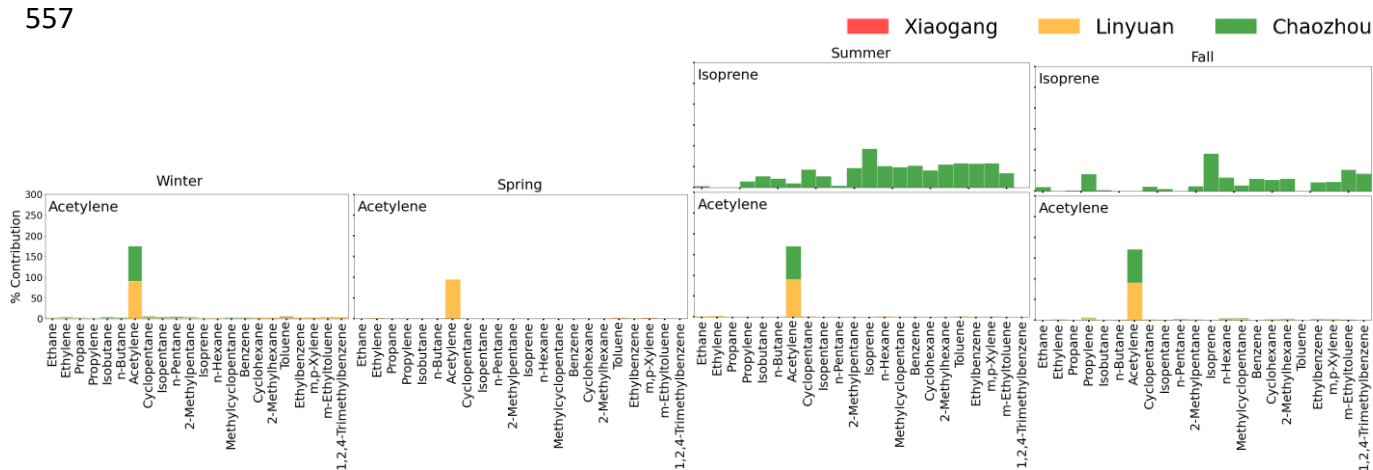
#### 535 a) Biogenic factor

536 The PMF results at Chaozhou identify a biogenic factor dominated by isoprene, with contributions  
537 present in both summer and fall (Fig.5). Temporal patterns (Fig. S7a,b) show that isoprene levels are  
538 substantially higher and more variable in summer, consistent with strong temperature and solar radiation  
539 dependence of biogenic isoprene emissions (Zeng et al., 2023; Vettikkat et al., 2023). These conditions  
540 are more intense and sustained during the summer months in southern Taiwan, and the surrounding  
541 agricultural landscape provides a plausible source. The pronounced late-morning to mid-afternoon peak  
542 (10:00–15:00) further supports a photosynthetically driven biogenic origin.

543 Notably, the biogenic factor profile also contains co-emitted VOCs, forming a mixed-species  
544 profile in which the isoprene signature is less distinct in summer but appears cleaner and more purely  
545 biogenic in fall. The observation is consistent with emerging evidence that urban isoprene budgets can  
546 include other non-biogenic sources (Peron et al., 2024), or traffic emissions (Chang et al., 2014; Hsieh  
547 et al., 2017). Residential biomass burning is another plausible contributor that can modify ambient  
548 mixtures during episodic events (Desservettaz et al., 2023). Given the agricultural setting at Chaozhou,  
549 biomass burning is likely a significant local source.

550 The CPF analysis (Fig. S7c) further supports a local and regionally distributed source profile, with  
551 increased conditional probabilities from the SSW and NW sectors during both seasons. These wind  
552 directions correspond with vegetated and agricultural areas surrounding the site, reinforcing the role of  
553 nearby land cover in influencing isoprene levels. However, the non-directional component and broader  
554 sector coverage also support additional inputs from anthropogenic sources, particularly traffic emissions  
555 and biomass burning. The seasonal and diurnal behaviors highlight the sensitivity of isoprene to  
556 environmental drivers and the complex nature of its mixed-source regions, such as Chaozhou.

557



559 **Figure 5:** Distinct source profiles of NMHC at the three sites in 2024

#### 560 b) Acetylene factor

561 Acetylene ( $C_2H_2$ ) is a highly flammable hydrocarbon gas and is mainly used as a fuel gas for oxy-  
562 acetylene welding, cutting, brazing, and soldering. On the other hand, the filling process for high-  
563 pressure cylinders is also prone to leaking. From the PMF results in Fig. 5, there is a resolved factor for

564 the single species of acetylene and no other accompanying species source at Linyuan and Chaozhou,  
565 suggesting that acetylene is a pronounced local source, which is consistent with the prior knowledge of  
566 the acetylene filling plant in the region.

567 PMF-resolved time series of the acetylene factor reveals a temporal pattern, with elevated  
568 contributions during winter and fall, and generally lower levels in summer (Fig. S5). These variations  
569 are likely driven by meteorological influences, such as enhanced atmospheric stability and reduced  
570 boundary layer height in colder months, which favor the accumulation of locally emitted pollutants. In  
571 contrast, stronger vertical mixing and photochemical degradation in summer likely contribute to the  
572 overall reduction in acetylene levels during this period.

573 Complementary insights are provided by the CPF analysis, which highlights the directional  
574 characteristics of acetylene sources. Seasonal CPF polar plots show that Linyuan (orange) consistently  
575 exhibits strong directional signals, with the highest probabilities originating from the NW–NE across  
576 all seasons. This directional consistency supports the presence of a persistent local source to the north  
577 of the site—aligned with the known location of an acetylene filling plant in the region. The elevated CPF  
578 values in these wind sectors reinforce the interpretation that the PMF-resolved acetylene factor reflects  
579 a geographically localized emission source, with its observed variability driven more by meteorological  
580 transport conditions than by changes in source activity. In contrast, no acetylene factor was resolved at  
581 Xiaogang, and this absence is consistent with its prevailing wind patterns. Seasonal wind rose data show  
582 that Xiaogang is predominantly influenced by W and NW winds (Fig. S8)—directions that do not align  
583 with the position of the acetylene source near Linyuan, which lies to the southeast of Xiaogang. As a  
584 result, the site remains largely unaffected by emissions from the filling facility.

585 Chaozhou is an agricultural area that leads to open-field biomass burning beginning in late summer  
586 and extending to the rest of the year. Acetylene is an emission from incomplete combustion processes,  
587 such as biomass burning (Burling et al., 2010; Wang et al., 2014), and therefore exhibits its strongest  
588 summer spikes and weaker, intermittent fall and winter contributions (Fig. 2a, Fig. S1). This seasonal  
589 pattern reflects intermittent but intensified combustion activities rather than continuous emissions.  
590 Consequently, although PMF resolves an acetylene-rich factor at both Linyuan and Chaozhou, its  
591 contribution at Chaozhou is much lower (Fig. S5). Unlike Linyuan—where a known nearby acetylene  
592 filling plant provides a persistent local source—Chaozhou is influenced mainly by diffuse biomass  
593 burning and other small-scale, variable combustion activities. The absence of a strong directional signal  
594 in the CPF analysis for Chaozhou further supports the interpretation that acetylene in Chaozhou  
595 originates from non-point or variable sources rather than a single dominant emitter.

### 596 **3.4 PMF-Trigger back trajectory integration**

597 It is noteworthy that an acetylene-related factor was clearly resolved in the PMF results, especially  
598 for Linyuan but not for Xiaogang. This outcome aligns well with the raw PAMS observations, where  
599 acetylene concentrations at Linyuan are markedly elevated, often exhibiting sharp spikes reaching  
600 several hundred ppb (Fig. S1), especially in winter. In contrast, levels at Xiaogang remain consistently  
601 low, rarely exceeding 20 ppb. The resolution of the acetylene factor at Linyuan can be attributed to the

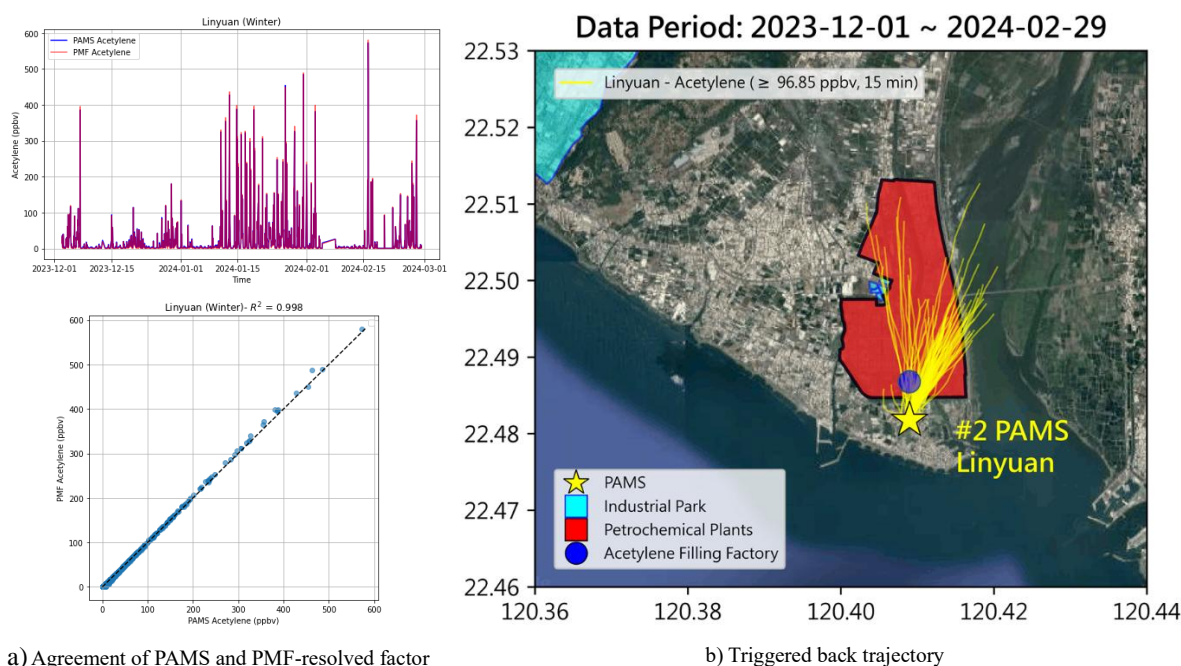
602 high signal-to-noise ratio in the PAMS data, where sharp and frequent concentration spikes provided a  
603 clear signal for PMF to distinguish this source from others, resulting in a well-defined temporal profile  
604 that closely matched the observed data. This supports the reliability of PMF in capturing source-specific  
605 signatures when driven by strong observational input.

606 Beyond factor profiles and species contributions, the PMF-resolved acetylene factor at Linyuan  
607 also resulted in a well-defined temporal profile that closely matched the observed data. Figure 6a  
608 demonstrates this consent with a coefficient of determination ( $R^2$ ) exceeding 0.99. This high level of  
609 agreement underscores the ability of PMF to cleanly resolve the profile dominated by a single species,  
610 acetylene, and to accurately reproduce the temporal variability of pollutant levels. While many PMF  
611 studies focus primarily on profile interpretation, this study demonstrates that time series validation can  
612 provide an additional, rigorous layer of confidence in the factor identification—highlighting the  
613 robustness of the PAMS dataset and the reliability of the PMF analysis. As a result, acetylene serves as  
614 an intrinsic reference species, providing an internal check on the PMF analysis.

615 Because the acetylene events at Linyuan are extremely distinct, a triggered back-trajectory  
616 analysis was conducted to investigate their source locations. This analysis used observational data from  
617 the monitoring station as input, under the assumption that the local wind field was representative of the  
618 broader surrounding area. The model was configured to calculate air parcel trajectories 15 minutes  
619 backward from the observation site. Geographic Information System (GIS) tools and Google Maps API  
620 were used to spatially visualize the trajectories and identify potential emission hotspots through  
621 trajectory receptor pattern overlay analysis. Setting an appropriate concentration threshold is critical for  
622 isolating representative pollution events. If the threshold is too low, resulting trajectories may be overly  
623 dispersed, making source identification difficult. Conversely, a threshold set too high may highlight  
624 only extreme events, which may not represent typical source behavior. This analysis applied a threshold  
625 of 96.85 ppb (95th quantile) to ensure that only significant acetylene events were considered.

626 The overlay of multiple high-concentration trajectories consistently pointed to an area near the  
627 acetylene filling facility (Fig. 6). Although the backward trajectories do not align perfectly with the  
628 suspected emission source, this deviation is likely due to the influence of complex coastal meteorology  
629 that can affect low-level air parcel paths, especially under transitional wind conditions. Moreover, the  
630 trajectory model may not fully capture local turbulence and terrain effects, contributing to the observed  
631 offset. Despite this, the temporal patterns of peaked acetylene, combined with the site's position relative  
632 to the dominant wind direction, support the likely influence of the identified source. These findings  
633 demonstrate the value of high-resolution PAMS data in capturing pollutant events and reinforce the  
634 consistency between observational measurements and PMF-based source apportionment. Finally, the  
635 back-trajectory method, particularly when applied in a triggered mode during elevated events, offers  
636 enhanced spatial resolution and source identification capabilities that complement and extend beyond  
637 PMF results. Further trajectories are also run for Chaozhou, which supports the hypothesis that the high  
638 peak in August originates from local sources, indicating an intermittent episode peak from biomass  
639 burning in such a highly agricultural landscape (Fig. S1). This interpretation is further strengthened by

640 the trajectory analysis (Fig. S9), which shows locally originating and spatially scattered air mass  
641 pathways around the monitoring site.



a) Agreement of PAMS and PMF-resolved factor

b) Triggered back trajectory

642 **Figure 6:** The acetylene factor at Linyuan, (a) time series comparison and (b) Triggered back trajectory  
643 analysis of spike levels. Base map from Google Maps (Map data ©2025 Google).

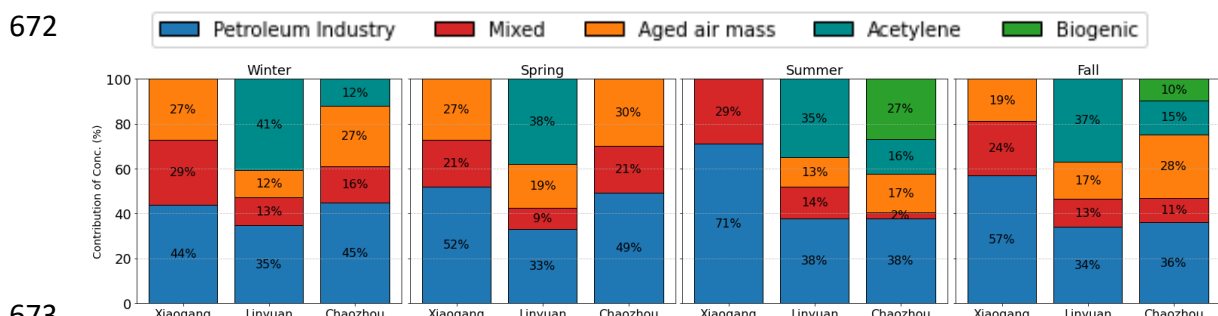
### 644 3.5 Quantitative estimates of source contributions.

645 The differences in source contribution across the three sites are not arbitrary but rather reflect the  
646 distinct roles each monitoring station plays within the regional emission landscape. Linyuan functions as  
647 a source site because it is home to major refinery and petrochemical facilities. Xiaogang, by contrast,  
648 presents a mixed urban-industrial environment, while Chaozhou acts as a downwind receptor site in a  
649 predominantly rural setting. Since many NMHC species originate from multiple source types, the  
650 resolved factors were grouped into broader categories: petroleum industry (including petro I & II,  
651 refinery, and industrial fugitive emissions), mixed, aged air mass, acetylene, and biogenic.

652 Figure 7 illustrates the seasonal contribution of these grouped sources. Interestingly, the petroleum-  
653 related source contribution is most prominent (33-71%), especially at Xiaogang, despite Linyuan being  
654 the location of core petrochemical activities. This apparent contradiction can be explained by local  
655 meteorological conditions—particularly prevailing winds and sea-land breeze effects—which frequently  
656 transport emissions from the surrounding industrial corridor toward Xiaogang. These wind-driven  
657 dynamics create a receptor-source relationship, wherein Xiaogang accumulates both locally emitted and  
658 regionally transported pollutants. In contrast, Linyuan shows a strong signal from the acetylene factor,  
659 pointing to localized activities with distinct point-source characteristics. Meanwhile, Chaozhou's  
660 elevated aged air mass contribution underscores its role as a downwind receptor site.

661 Aged air masses consistently influence all sites and seasons, with contributions ranging from 12%  
662 to 30%. Chaozhou, in particular, exhibits higher contributions—up to 30% in spring and above 27% in  
663 winter and fall, while summer shows the lowest levels. Its inland, rural settings with limited local

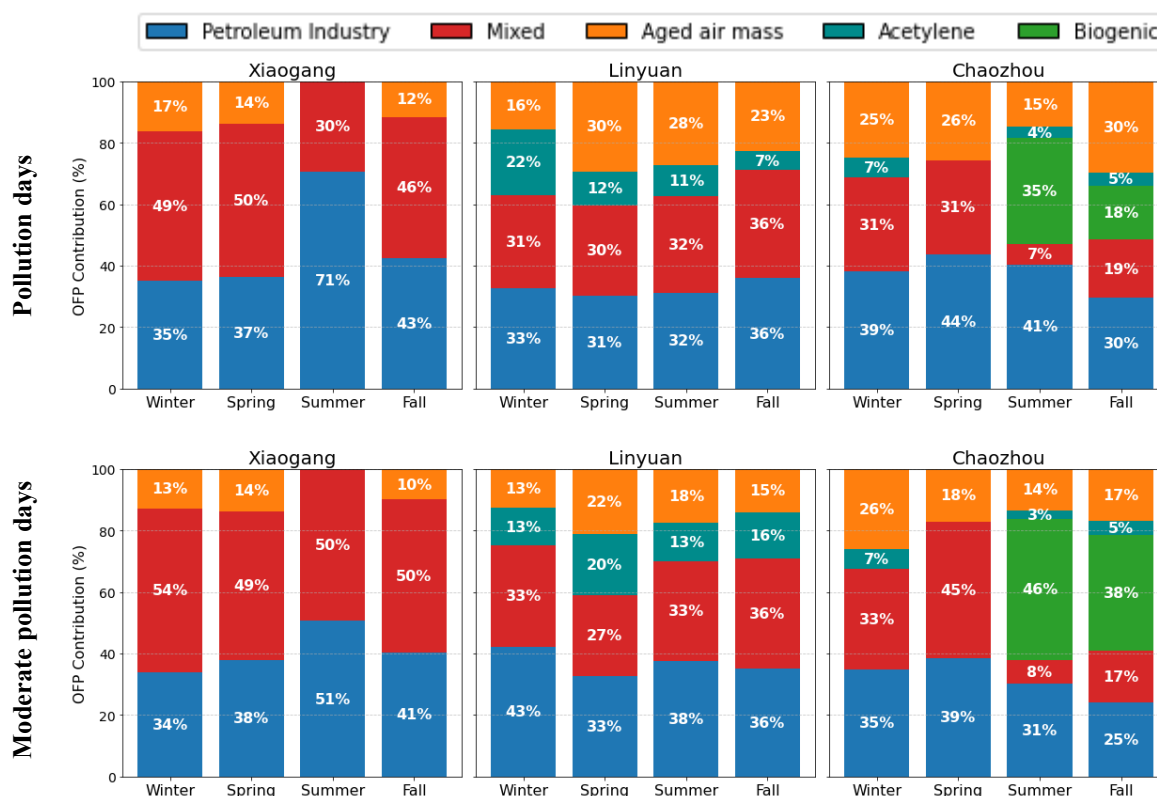
664 industrial activity suggest that the site primarily receives aged air masses transported from upwind  
 665 regions. Supporting this interpretation, evidence from CPF analysis (Fig. 4 and Fig. S6) highlights the  
 666 role of local recirculation driven by sea-land breeze, which enhances the aging of air masses near the site.  
 667 Additionally, long-range transport under prevailing winter monsoon winds further reinforces the elevated  
 668 aged air signal observed at Chaozhou. At the same time, Xiaogang emerged as the second contributor of  
 669 aged air mass, with notable peaks in winter, spring, and fall. As a result, the three sites with their unique  
 670 source-receptor characteristics produce very dynamic source apportionment results that vary in season  
 671 and locations.



673  
 674 **Figure 7:** Seasonal contributions of grouped source factors at each site. Details of the eight resolved  
 675 factors are provided in Fig. S10

676 **3.6 OFP dynamics under varying ozone conditions**

677 Given that photochemical reactions predominantly occur during daylight hours, the OFP was  
 678 calculated exclusively for daytime periods, defined using sunrise and sunset times, derived from  
 679 astronomical data tailored to each station's geographic locations and observation dates. Seasonally  
 680 averaged OFP values attributed to source factors were highest at Xiaogang ( $113.20 \pm 23.60 \mu\text{g}/\text{m}^3$ ),  
 681 followed by Linyuan ( $102.73 \pm 40.93 \mu\text{g}/\text{m}^3$ ), and lowest at Chaozhou ( $65.38 \pm 9.00 \mu\text{g}/\text{m}^3$ ), as shown  
 682 in Fig. S11. Spatially, the distribution of OFP contributions varied consistently with their previously  
 683 identified roles. Notably, while petroleum-related sources exhibited the highest contributions in terms  
 684 of concentration, they were not always the leading contributors to OFP. For example, at Xiaogang, the  
 685 petroleum factor ranked second in OFP, overtaken by the mixed source factor (Fig. S11). This is  
 686 primarily due to the presence of highly reactive species—such as aromatics—in the mixed source profile,  
 687 which significantly elevates its OFP despite relatively lower concentrations. In Xiaogang, the mixed  
 688 source was the dominant contributor to OFP during most seasons, with petroleum-related sources only  
 689 surpassing it in summer. To further explore source contributions under varying ozone pollution  
 690 conditions, the dataset was classified based on the maximum daily 8-hour average (MDA8) ozone  
 691 concentrations: days with MDA8 larger than 60 ppb were designated as pollution (POL) days, and those  
 692 with MDA8 between 40 and 60 ppb as moderate pollution (MOD) days. OFP was recalculated  
 693 accordingly, and the percentage contributions of each source factor are presented in Figure 8. The  
 694 comparison between POL and MOD days reveals notable shifts in source influence across the region.



695 **Figure 8:** Corresponding daytime OFP during pollution and moderate pollution days of ozone

696 Mixed and petroleum-related sources consistently contribute a substantial portion of OFP under  
 697 both conditions. For example, mixed sources are the dominant contributor, particularly at urban-  
 698 industrial sites such as Xiaogang, underscoring their strong role in ozone precursor formation even  
 699 during less intense ozone conditions. Meanwhile, petroleum-related sources showed an enhanced  
 700 contribution at Linyuan, suggesting a stronger association with moderate ozone levels. Overall, large-  
 701 scale industrial and traffic-related emissions (petro-, mixed, and acetylene-related) provide a highly  
 702 reactive precursor condition conducive to ozone formation across Xiaogang and Linyuan areas,  
 703 consistent with their dense industrial landscape.

704 Under moderate-ozone conditions, the mixed-source factor contributes the largest share of OFP.  
 705 These episodes are frequently associated with lower wind speeds and reduced mixing heights (Aacog,  
 706 2015), favoring the accumulation of locally emitted species from traffic, solvents, and smaller-scale  
 707 industrial activities. The coexistence of these emissions provides a balanced supply of reactive aromatics  
 708 and olefins, sustaining ozone production even in the absence of strong photochemical aging. This pattern  
 709 reflects the VOC-limited photochemical environment prevalent in southern Taiwan, where ozone  
 710 formation is more sensitive to reactive VOCs than to NO<sub>x</sub> levels (Chang et al., 2022), emphasizing that  
 711 moderate-ozone episodes are primarily governed by local accumulation and NMHC composition.  
 712 However, the mixed-source factor reflects overlapping characteristics of vehicular and solvent-related  
 713 species. This incomplete separation introduces some uncertainty in source-specific attribution of OFP.  
 714 Nevertheless, this overlap mirrors the reality of urban environments.

715 Meanwhile, the aged air mass factor exerted a notable influence on ozone pollution days,  
 716 especially at downwind sites such as Linyuan and Chaozhou. This highlights the role of regional

717 transport and atmospheric aging in shaping local ozone levels. The elevated OFP from aged air mass  
718 during pollution events suggests that some reactive NMHCs are transported from upwind areas after  
719 undergoing photochemical processing rather than being emitted locally. Importantly, aged air masses  
720 may also carry ozone itself, effectively elevating the background ozone concentration and providing a  
721 higher baseline upon which local photochemical production builds (Nguyen et al., 2025). This dual  
722 role—delivering both precursors and ozone—can intensify pollution episodes.

723 At Chaozhou, biogenic emissions made a significant contribution to the OFP, particularly during  
724 the summer and fall seasons. This reflects the release of isoprene from surrounding agriculture and  
725 vegetation landscape, which can react rapidly with transported NO<sub>x</sub> to form ozone. The biogenic  
726 influence was especially evident during moderate ozone days, suggesting that these episodes are more  
727 sensitive to the combined effects of natural emissions, transported NO<sub>x</sub>, and local atmospheric  
728 chemistry. This underscores the importance of considering seasonal and spatial dynamics in emission  
729 control strategies—especially in areas like Xiaogang and Linyuan, where anthropogenic and biogenic  
730 sources interact synergistically to elevate ozone levels.

731 Regarding chemical speciation, the dominant OFP contributors across all sites and seasons were  
732 aromatics, alkanes, and alkenes, owing to their high photochemical reactivity. Aromatics—particularly  
733 toluene and m,p-xylene (Fig. S12)—accounted for 32–61% of the OFP during moderate pollution days,  
734 with the highest contributions observed at Xiaogang. Alkanes, primarily ethane, contributed 20–35%,  
735 with similar levels at Xiaogang and Linyuan, and slightly higher at Chaozhou during polluted periods.  
736 Alkenes, especially propylene, contributed 15–24%, peaking at Xiaogang during pollution days and at  
737 Linyuan during moderate ozone conditions. Additional contributions were observed from ethyne—  
738 notably at Linyuan—and from isoprene at Chaozhou, where they played a more prominent role under  
739 moderate ozone conditions. Although acetylene has a relatively low MIR value, its large emission  
740 volume—primarily from the filling plant—still led to significant OPF contribution downwind.

741 The persistence of higher OFP contributions during moderate ozone days indicates that precursor  
742 control should not be limited to pollution events alone. Effective ozone management, therefore, requires  
743 a multi-faceted approach that integrates anthropogenic and biogenic sources, seasonal variability, and  
744 transportation influences to design more adaptive, location-specific mitigation policies.

#### 745 **4. Conclusion**

746 This study provides a comprehensive analysis of NMHC concentrations and their sources across  
747 three distinct sites in southern Taiwan: Linyuan, Xiaogang, and Chaozhou. The findings revealed  
748 significant spatial heterogeneity in NMHC concentrations and source profiles, reflecting the diverse  
749 land use and industrial activities across the region. Linyuan, a dense industrial landscape, exhibited the  
750 highest average NMHC concentrations, followed by the mixed urban-industrial environment of  
751 Xiaogang, with the lowest levels observed at the predominantly agricultural site of Chaozhou. PMF  
752 analysis identified eight distinct source factors contributing to NMHCs at the three sites: petrochemical  
753 I & II, refinery, industrial fugitive emissions, mixed (vehicular/solvent), aged air mass, acetylene, and  
754 biogenic.

755 The strength of this study lies in the use of PMF-resolved time series output, allowing for the  
756 identification of concentration spikes indicative of episodic emission events. The acetylene factor, in  
757 particular, showed excellent agreement with PAMS observations ( $R^2$  over 0.99), which triggered  
758 targeted back-trajectory analyses. These consistently traced emissions to a nearby acetylene filling  
759 facility north of the Linyuan industrial area. The integration of PMF-resolved time series data with  
760 trajectory modeling reinforces the credibility of the source apportionment results and underscores the  
761 high quality and temporal resolution of the observational data. It enabled a more precise attribution of  
762 pollution sources and facilitated the isolation and examination of individual pollution events.

763 In addition, this study explored the dynamics of OFP. They were calculated specifically for  
764 daytime periods—when photochemical activity is most pronounced. Seasonally averaged OFP was  
765 highest at Xiaogang ( $113.20 \pm 23.60 \mu\text{g}/\text{m}^3$ ), followed by Linyuan ( $102.73 \pm 40.93 \mu\text{g}/\text{m}^3$ ), and lowest  
766 at the downwind rural site Chaozhou ( $65.38 \pm 9.00 \mu\text{g}/\text{m}^3$ ). Although petroleum-related sources  
767 contributed the largest fraction of NMHC concentrations, the mixed source factor—enriched in highly  
768 reactive species such as aromatics and olefins—often dominates the OFP, particularly at Xiaogang.  
769 Under moderate-ozone conditions (MDA8 40–60 ppb), the factor became the principal driver of ozone  
770 formation, consistent with local accumulation under stagnant meteorological conditions and limited  
771 vertical mixing. The coexistence of both reactive aromatics and olefins within this factor sustained  
772 ozone production despite weak photochemical aging, reflecting a VOC-limited regime typical of  
773 southern Taiwan. Across ozone pollution levels, petroleum and mixed sources remained dominant, but  
774 their relative influence varied with site characteristics. Mixed sources exerted stronger effects during  
775 moderate-ozone episodes at urban–industrial locations, whereas petroleum-related sources dominated  
776 in Linyuan under similar conditions. These results suggest that frequent, moderate-ozone episodes are  
777 primarily driven by locally accumulated reactive NMHCs. This pattern may also reflect the early  
778 impacts of emission control measures, which are more effective under high-pollution conditions but less  
779 so during moderate episodes. Given their higher occurrence, moderate pollution episodes still offer  
780 valuable insights into the interplay between local accumulation, VOC reactivity, and emission  
781 composition that governs ozone formation in the region.

782 Overall, this study demonstrates the strength of a refined source apportionment approach using  
783 multi-site, year-round, high-frequency NMHC measurements, each reflecting distinct source–receptor  
784 dynamics. The findings offer a more comprehensive spatiotemporal understanding of ozone formation  
785 mechanisms and provide a scientific basis for coordinated control of mobile, solvent-related, and  
786 petroleum-associated emissions across southern Taiwan.

787 **Data availability:** All raw data can be provided by the corresponding authors upon request.

788 **Author contributions:** JLW and CHW formed the conceptualization; HCH developed the model code  
789 and performed the modeling; DHN and HCH analyzed the data; DHN wrote the original draft; JLW,  
790 NHL, CHW, MCL, and DHN reviewed and edited the manuscript.

791 **Competing interests:** The authors declare that they have no conflict of interest.

## 792 **References**

793 AACOG: Conceptual Model, Ozone Analysis of the San Antonio Region, Updates through Year 2014,

794 [https://aacog.gov/sites/default/files/2022-](https://aacog.gov/sites/default/files/2022-07/Conceptual%20Model%2C%20Ozone%20Analysis%20of%20the%20San%20Antonio%20Region%2C%20Updates%20through%20Year%202014.pdf?utm_source=chatgpt.com)  
795 [07/Conceptual%20Model%2C%20Ozone%20Analysis%20of%20the%20San%20Antonio%20Region](https://aacog.gov/sites/default/files/2022-07/Conceptual%20Model%2C%20Ozone%20Analysis%20of%20the%20San%20Antonio%20Region%2C%20Updates%20through%20Year%202014.pdf?utm_source=chatgpt.com)  
796 [%2C%20Updates%20through%20Year%202014.pdf?utm\\_source=chatgpt.com](https://aacog.gov/sites/default/files/2022-07/Conceptual%20Model%2C%20Ozone%20Analysis%20of%20the%20San%20Antonio%20Region%2C%20Updates%20through%20Year%202014.pdf?utm_source=chatgpt.com), 2015.  
797 Atkinson, R.: Kinetics and mechanisms of the gas-phase reactions of the hydroxyl radical with organic  
798 compounds under atmospheric conditions, *Chemical Reviews*, 86, 69-201, 1986.  
799 Atkinson, R. and Arey, J.: Atmospheric degradation of volatile organic compounds, *Chemical reviews*,  
800 103, 4605-4638, <https://pubs.acs.org/doi/full/10.1021/cr0206420>, 2003.  
801 Baidar, S., Hardesty, R., Kim, S. W., Langford, A., Oetjen, H., Senff, C., Trainer, M., and Volkamer, R.:  
802 Weakening of the weekend ozone effect over California's South Coast Air Basin, *Geophysical Research*  
803 *Letters*, 42, 9457-9464, <https://doi.org/10.1002/2015GL066419>, 2015.  
804 Baker, A. K., Beyersdorf, A. J., Doezema, L. A., Katzenstein, A., Meinardi, S., Simpson, I. J., Blake, D.  
805 R., and Rowland, F. S.: Measurements of nonmethane hydrocarbons in 28 United States cities,  
806 *Atmospheric Environment*, 42, 170-182, <https://doi.org/10.1016/j.atmosenv.2007.09.007>, 2008.  
807 Bari, M. A. and Kindzierski, W. B.: Ambient volatile organic compounds (VOCs) in Calgary, Alberta:  
808 sources and screening health risk assessment, *Science of the Total Environment*, 631, 627-640,  
809 <https://doi.org/10.1016/j.scitotenv.2018.03.023>, 2018.  
810 Bourtsoukidis, E., Ernle, L., Crowley, J. N., Lelieveld, J., Paris, J.-D., Pozzer, A., Walter, D., and  
811 Williams, J.: Non-methane hydrocarbon (C 2–C 8) sources and sinks around the Arabian Peninsula,  
812 *Atmospheric Chemistry Physics*, 19, 7209-7232, 2019.  
813 Burling, I., Yokelson, R. J., Griffith, D. W., Johnson, T. J., Veres, P., Roberts, J., Warneke, C., Urbanski,  
814 S., Reardon, J., and Weise, D.: Laboratory measurements of trace gas emissions from biomass burning  
815 of fuel types from the southeastern and southwestern United States, *Atmospheric Chemistry Physics*, 10,  
816 11115-11130, 2010.  
817 Buzcu, B. and Fraser, M. P.: Source identification and apportionment of volatile organic compounds in  
818 Houston, TX, *Atmospheric Environment*, 40, 2385-2400,  
819 <https://doi.org/10.1016/j.atmosenv.2005.12.020>, 2006.  
820 Cai, C., Geng, F., Tie, X., Yu, Q., and An, J.: Characteristics and source apportionment of VOCs measured  
821 in Shanghai, China, *Atmospheric Environment*, 44, 5005-5014,  
822 <https://doi.org/10.1016/j.atmosenv.2010.07.059>, 2010.  
823 Carter, W. P.: Development of the SAPRC-07 chemical mechanism, *Atmospheric Environment*, 44,  
824 5324-5335, <https://doi.org/10.1016/j.atmosenv.2010.01.026>, 2010.  
825 Chang, C.-C., Chen, T.-Y., Chou, C., and Liu, S.-C.: Assessment of traffic contribution to hydrocarbons  
826 using 2, 2-dimethylbutane as a vehicular indicator, *Terrestrial Atmospheric Oceanic Sciences*, 15, 697-  
827 712, 2004.  
828 Chang, C.-C., Lo, S.-J., Lo, J.-G., and Wang, J.-L.: Analysis of methyl tert-butyl ether in the atmosphere  
829 and implications as an exclusive indicator of automobile exhaust, *Atmospheric Environment*, 37, 4747-  
830 4755, <https://doi.org/10.1016/j.atmosenv.2003.08.017>, 2003.  
831 Chang, C.-C., Wang, J.-L., Lung, S.-C. C., Chang, C.-Y., Lee, P.-J., Chew, C., Liao, W.-C., Chen, W.-N.,

832 and Ou-Yang, C.-F.: Seasonal characteristics of biogenic and anthropogenic isoprene in tropical–  
833 subtropical urban environments, *Atmospheric environment*, 99, 298-308,  
834 <https://doi.org/10.1016/j.atmosenv.2014.09.019>, 2014.

835 Chang, J. H.-W., Griffith, S. M., Kong, S. S.-K., Chuang, M.-T., and Lin, N.-H.: Development of a  
836 CMAQ-PMF-based composite index for prescribing an effective ozone abatement strategy: A case study  
837 of sensitivity of surface ozone to precursor VOC species in southern Taiwan, *Atmospheric Chemistry  
838 Physics Discussions*, 2022, 1-48, <https://doi.org/10.5194/acp-23-6357-2023>, 2022.

839 Chen, C.-H., Chuang, Y.-C., Hsieh, C.-C., and Lee, C.-S.: VOC characteristics and source apportionment  
840 at a PAMS site near an industrial complex in central Taiwan, *Atmospheric Pollution Research*, 10, 1060-  
841 1074, 2019.

842 Chen, C., Wang, L., Qin, Y., Zhang, Y., Zheng, S., Yang, Y., Jin, S., and Yang, X.: Voc characteristics and  
843 their source apportionment in the yangtze river delta region during the g20 summit, *Atmosphere*, 12, 928,  
844 <https://doi.org/10.3390/atmos12070928>, 2021a.

845 Chen, S.-P., Liu, W.-T., Hsieh, H.-C., and Wang, J.-L.: Taiwan ozone trend in response to reduced  
846 domestic precursors and perennial transboundary influence, *Environmental Pollution*, 289, 117883,  
847 <https://doi.org/10.1016/j.envpol.2021.117883>, 2021b.

848 Chen, S.-P., Liu, T.-H., Chen, T.-F., Yang, C.-F. O., Wang, J.-L., and Chang, J. S.: Diagnostic modeling  
849 of PAMS VOC observation, *Environmental Science Technology*, 44, 4635-4644,  
850 <https://doi.org/10.1021/es903361r>, 2010.

851 Chen, S.-P., Liao, W.-C., Chang, C.-C., Su, Y.-C., Tong, Y.-H., Chang, J. S., and Wang, J.-L.: Network  
852 monitoring of speciated vs. total non-methane hydrocarbon measurements, *Atmospheric Environment*,  
853 90, 33-42, 2014.

854 Cheng, J.-O., Ko, F.-C., Lee, C.-L., and Fang, M.-D.: Atmospheric polycyclic aromatic hydrocarbons  
855 (PAHs) of southern Taiwan in relation to monsoons, *Environmental Science Pollution Research*, 23,  
856 15675-15688, <https://doi.org/10.1007/s11356-016-6751-9>, 2016.

857 Chou, C. C. K., Lung, S.-C. C., Hsiao, T.-C., and Lee, C.-T.: Regional and Urban Air Quality in East  
858 Asia: Taiwan, in: *Handbook of Air Quality and Climate Change*, 1-38, [https://doi.org/10.1007/978-981-  
15-2527-8\\_71-1](https://doi.org/10.1007/978-981-<br/>859 15-2527-8_71-1), 2022.

860 Deng, Y.-M., Wu, H.-W., and Liao, H.-E.: Utilization intention of community pharmacy service under  
861 the dual threats of air pollution and COVID-19 epidemic: Moderating effects of knowledge and attitude  
862 toward COVID-19, *International Journal of Environmental Research Public Health*, 19, 3744,  
863 <https://doi.org/10.3390/ijerph19063744>, 2022.

864 Desservettaz, M., Pikridas, M., Stavroulas, I., Bougiatioti, A., Liakakou, E., Hatzianastassiou, N., Sciare,  
865 J., Mihalopoulos, N., and Bourtsoukidis, E.: Emission of volatile organic compounds from residential  
866 biomass burning and their rapid chemical transformations, *Science of The Total Environment*, 903,  
867 166592, 2023.

868 Dong, Z., Zhang, D., Wang, T., Song, X., Hao, Y., Wang, S., and Wang, S.: Sources and environmental  
869 impacts of volatile organic components in a street canyon: Implication for vehicle emission, *Science of*

870 The Total Environment, 917, 170569, <https://doi.org/10.1016/j.scitotenv.2024.170569>, 2024.

871 Dumanoglu, Y., Kara, M., Altiok, H., Odabasi, M., Elbir, T., and Bayram, A.: Spatial and seasonal  
872 variation and source apportionment of volatile organic compounds (VOCs) in a heavily industrialized  
873 region, Atmospheric Environment, 98, 168-178, <https://doi.org/10.1016/j.atmosenv.2014.08.048>, 2014.

874 Finlayson-Pitts, B. and Pitts Jr, J.: Atmospheric chemistry of tropospheric ozone formation: scientific  
875 and regulatory implications, Air Waste, 43, 1091-1100, 1993.

876 Gentner, D. R., Harley, R. A., Miller, A. M., and Goldstein, A. H.: Diurnal and seasonal variability of  
877 gasoline-related volatile organic compound emissions in Riverside, California, Environmental Science  
878 Technology, 43, 4247-4252, 2009.

879 Gilman, J. B., Lerner, B. M., Kuster, W. C., and De Gouw, J.: Source signature of volatile organic  
880 compounds from oil and natural gas operations in northeastern Colorado, Environmental Science  
881 Technology, 47, 1297-1305, 2013.

882 Gilman, J. B., Burkhardt, J. F., Lerner, B. M., Williams, E. J., Kuster, W., Goldan, P. D., Murphy, P. C.,  
883 Warneke, C., Fowler, C., and Montzka, S. A.: Ozone variability and halogen oxidation within the Arctic  
884 and sub-Arctic springtime boundary layer, Atmospheric Chemistry Physics, 10, 10223-10236, 2010.

885 Gu, Y., Liu, B., Li, Y., Zhang, Y., Bi, X., Wu, J., Song, C., Dai, Q., Han, Y., and Ren, G.: Multi-scale  
886 volatile organic compound (VOC) source apportionment in Tianjin, China, using a receptor model  
887 coupled with 1-hr resolution data, Environmental Pollution, 265, 115023,  
888 <https://doi.org/10.1016/j.envpol.2020.115023>, 2020.

889 Guan, Y., Wang, L., Wang, S., Zhang, Y., Xiao, J., Wang, X., Duan, E., and Hou, L. a.: Temporal  
890 variations and source apportionment of volatile organic compounds at an urban site in Shijiazhuang,  
891 China, Journal of Environmental Sciences, 97, 25-34, <https://doi.org/10.1016/j.jes.2020.04.022>, 2020.

892 Guo, H., Cheng, H., Ling, Z., Louie, P., and Ayoko, G.: Which emission sources are responsible for the  
893 volatile organic compounds in the atmosphere of Pearl River Delta?, Journal of Hazardous Materials,  
894 188, 116-124, <https://doi.org/10.1016/j.jhazmat.2011.01.081>, 2011.

895 Guo, H., Ling, Z., Cheng, H., Simpson, I., Lyu, X., Wang, X., Shao, M., Lu, H., Ayoko, G., and Zhang,  
896 Y.: Tropospheric volatile organic compounds in China, Science of The Total Environment, 574, 1021-  
897 1043, <https://doi.org/10.1016/j.scitotenv.2016.09.116>, 2017.

898 Han, Y., Wang, T., Li, R., Fu, H., Duan, Y., Gao, S., Zhang, L., and Chen, J.: Measurement report: Volatile  
899 organic compound characteristics of the different land-use types in Shanghai: spatiotemporal variation,  
900 source apportionment and impact on secondary formations of ozone and aerosol, Atmospheric Chemistry  
901 and Physics, 23, 2877-2900, <https://doi.org/10.5194/acp-23-2877-2023>, 2023.

902 Henry, R. F.: Weekday/weekend differences in gasoline related hydrocarbons at coastal PAMS sites due  
903 to recreational boating, Atmospheric Environment, 75, 58-65,  
904 <https://doi.org/10.1016/j.atmosenv.2013.03.053>, 2013.

905 Hsieh, H.-C., Ou-Yang, C.-F., and Wang, J.-L.: Revelation of coupling biogenic with anthropogenic  
906 isoprene by highly time-resolved observations, Aerosol Air Quality Research, 17, 721-729,  
907 <https://doi.org/10.4209/aaqr.2016.04.0133>, 2017.

908 Huang, Y. S. and Hsieh, C. C.: Ambient volatile organic compound presence in the highly urbanized city:  
909 source apportionment and emission position, *Atmospheric Environment*, 206, 45-59,  
910 <https://doi.org/10.1016/j.atmosenv.2019.02.046>, 2019.

911 Hui, L., Liu, X., Tan, Q., Feng, M., An, J., Qu, Y., Zhang, Y., and Jiang, M.: Characteristics, source  
912 apportionment and contribution of VOCs to ozone formation in Wuhan, Central China, *Atmospheric  
913 Environment*, 192, 55-71, <https://doi.org/10.1016/j.atmosenv.2018.08.042>, 2018.

914 Jung, U. and Choi, S.-S.: Variation in abundance ratio of isoprene and dipentene produced from wear  
915 particles composed of natural rubber by pyrolysis depending on the particle size and thermal aging,  
916 *Polymers*, 15, 929, <https://doi.org/10.3390/polym15040929>, 2023.

917 Kim, E., Brown, S. G., Hafner, H. R., and Hopke, P. K.: Characterization of non-methane volatile organic  
918 compounds sources in Houston during 2001 using positive matrix factorization, *Atmospheric  
919 Environment*, 39, 5934-5946, <https://doi.org/10.1016/j.atmosenv.2005.06.045>, 2005.

920 Kleinman, L. I., Daum, P. H., Lee, Y. N., Nunnermacker, L. J., Springston, S. R., Weinstein-Lloyd, J.,  
921 and Rudolph, J.: Ozone production efficiency in an urban area, *Journal of Geophysical Research:  
922 Atmospheres*, 107, ACH 23-21-ACH 23-12, <https://doi.org/10.1029/2002JD002529>, 2002.

923 Ko, Y.-C.: Air Pollution and Its Health Effects on Residents in Taiwanese Communities, *The Kaohsiung  
924 Journal of Medical Sciences*, 12, 657-699, <https://doi.org/10.6452/kjms.199612.0657>, 1996.

925 Kumar, A., Sinha, V., Shabin, M., Hakkim, H., Bonsang, B., and Gros, V.: Non-methane hydrocarbon  
926 (NMHC) fingerprints of major urban and agricultural emission sources for use in source apportionment  
927 studies, *Atmospheric Chemistry Physics*, 20, 12133-12152, 2020.

928 Kuo, C.-P., Liao, H.-T., Chou, C. C.-K., and Wu, C.-F.: Source apportionment of particulate matter and  
929 selected volatile organic compounds with multiple time resolution data, *Science of the Total Environment*,  
930 472, 880-887, 2014.

931 Languille, B., Gros, V., Petit, J.-E., Honoré, C., Baudic, A., Perrussel, O., Foret, G., Michoud, V., Truong,  
932 F., and Bonnaire, N.: Wood burning: A major source of Volatile Organic Compounds during wintertime  
933 in the Paris region, *Science of The Total Environment*, 711, 135055,  
934 <https://doi.org/10.1016/j.scitotenv.2019.135055>, 2020.

935 Lau, A. K. H., Yuan, Z., Yu, J. Z., and Louie, P. K.: Source apportionment of ambient volatile organic  
936 compounds in Hong Kong, *Science of the total environment*, 408, 4138-4149,  
937 <https://doi.org/10.1016/j.scitotenv.2010.05.025>, 2010.

938 Leuchner, M. and Rappenglück, B.: VOC source-receptor relationships in Houston during TexAQS-II,  
939 *Atmospheric Environment*, 44, 4056-4067, <https://doi.org/10.1016/j.atmosenv.2009.02.029>, 2010.

940 Li, C., Liu, Y., Cheng, B., Zhang, Y., Liu, X., Qu, Y., An, J., Kong, L., Zhang, Y., and Zhang, C.: A  
941 comprehensive investigation on volatile organic compounds (VOCs) in 2018 in Beijing, China:  
942 Characteristics, sources and behaviours in response to O<sub>3</sub> formation, *Science of the Total Environment*,  
943 806, 150247, <https://doi.org/10.1016/j.scitotenv.2021.150247>, 2022.

944 Li, J., Xie, S., Zeng, L., Li, L., Li, Y., and Wu, R.: Characterization of ambient volatile organic  
945 compounds and their sources in Beijing, before, during, and after Asia-Pacific Economic Cooperation

946 China 2014, *Atmospheric Chemistry and Physics*, 15, 7945-7959, [https://doi.org/10.5194/acp-15-7945-](https://doi.org/10.5194/acp-15-7945-2015)  
947 [2015](https://doi.org/10.5194/acp-15-7945-2015), 2015.

948 Li, K., Jacob, D. J., Liao, H., Shen, L., Zhang, Q., and Bates, K. H.: Anthropogenic drivers of 2013–2017  
949 trends in summer surface ozone in China, *Proceedings of the National Academy of Sciences*, 422-427,

950 Li, L. and Wang, X.: Seasonal and diurnal variations of atmospheric non-methane hydrocarbons in  
951 Guangzhou, China, *Int J Environ Res Public Health*, 9, 1859-1873,  
952 <https://doi.org/10.3390/ijerph9051859>, 2012.

953 Liao, H.-T., Yen, C.-M., Chen, Y.-R., Wu, J.-D., Tsai, S.-W., and Wu, C.-F.: Vertical variation of source-  
954 apportioned PM<sub>2.5</sub> and selected volatile organic compounds near an elevated expressway in an urban  
955 area, *Environmental Science Pollution Research*, 31, 20477-20487, 2024.

956 Liao, H.-T., Yau, Y.-C., Huang, C.-S., Chen, N., Chow, J. C., Watson, J. G., Tsai, S.-W., Chou, C. C.-K.,  
957 and Wu, C.-F.: Source apportionment of urban air pollutants using constrained receptor models with a  
958 priori profile information, *Environmental Pollution*, 227, 323-333, 2017.

959 Lin, C.-W., Chiang, S.-B., and Lu, S.-J.: Investigation of MTBE and aromatic compound concentrations  
960 at a gas service station, *Environmental Monitoring Assessment*, 105, 327-339, 2005.

961 Lin, C.-Y., Wang, Z., Chou, C. C. K., Chang, C.-C., and Liu, S. C.: A numerical study of an autumn high  
962 ozone episode over southwestern Taiwan, *Atmospheric Environment*, 41, 3684-3701,  
963 <https://doi.org/10.1016/j.atmosenv.2006.12.050>, 2007.

964 Lingwall, J. W. and Christensen, W. F.: Pollution source apportionment using a priori information and  
965 positive matrix factorization, *Chemometrics Intelligent Laboratory Systems*, 87, 281-294,  
966 <https://doi.org/10.1016/j.chemolab.2007.03.007>, 2007.

967 Liu, Y., Shao, M., Fu, L., Lu, S., Zeng, L., and Tang, D.: Source profiles of volatile organic compounds  
968 (VOCs) measured in China: Part I, *Atmospheric Environment*, 42, 6247-6260,  
969 <https://doi.org/10.1016/j.atmosenv.2008.01.070>, 2008a.

970 Liu, Y., Shao, M., Lu, S., Chang, C.-C., Wang, J.-L., and Fu, L.: Source apportionment of ambient volatile  
971 organic compounds in the Pearl River Delta, China: Part II, *Atmospheric Environment*, 42, 6261-6274,  
972 <https://doi.org/10.1016/j.atmosenv.2008.02.027>, 2008b.

973 McFiggans, G., Mentel, T. F., Wildt, J., Pullinen, I., Kang, S., Kleist, E., Schmitt, S., Springer, M.,  
974 Tillmann, R., and Wu, C.: Secondary organic aerosol reduced by mixture of atmospheric vapours, *Nature*,  
975 565, 587-593, <https://doi.org/10.1038/s41586-018-0871-y>, 2019.

976 Mo, Z., Shao, M., Lu, S., Niu, H., Zhou, M., and Sun, J.: Characterization of non-methane hydrocarbons  
977 and their sources in an industrialized coastal city, Yangtze River Delta, China, *Science of the Total*  
978 *Environment*, 593, 641-653, <https://doi.org/10.1016/j.scitotenv.2017.03.123>, 2017.

979 Mo, Z., Shao, M., Lu, S., Qu, H., Zhou, M., Sun, J., and Gou, B.: Process-specific emission characteristics  
980 of volatile organic compounds (VOCs) from petrochemical facilities in the Yangtze River Delta, China,  
981 *Science of the Total Environment*, 533, 422-431, <https://doi.org/10.1016/j.scitotenv.2015.06.089>, 2015.

982 Implementation of Air Pollution Control Plan Achieves Remarkable Results, last access: 2025-12-04.

983 Latest Air Pollution Inventory Shows 19% Reduction Compared to Last Edition, last access: 2025-12-

984 04.

985 Na, K. and Kim, Y. P.: Chemical mass balance receptor model applied to ambient C<sub>2</sub>–C<sub>9</sub> VOC  
986 concentration in Seoul, Korea: effect of chemical reaction losses, *Atmospheric Environment*, 41, 6715-  
987 6728, <https://doi.org/10.1016/j.atmosenv.2007.04.054>, 2007.

988 Nakashima, Y., Kamei, N., Kobayashi, S., and Kajii, Y.: Total OH reactivity and VOC analyses for  
989 gasoline vehicular exhaust with a chassis dynamometer, *Atmospheric Environment*, 44, 468-475,  
990 <https://doi.org/10.1016/j.atmosenv.2009.11.006>, 2010.

991 Nelson, P. and Quigley, S.: The hydrocarbon composition of exhaust emitted from gasoline fuelled  
992 vehicles, *Atmospheric Environment*, 18, 79-87, [https://doi.org/10.1016/0004-6981\(84\)90230-0](https://doi.org/10.1016/0004-6981(84)90230-0), 1984.

993 Nguyen, D. H., Hsieh, H. C., Chen, S. P., Ou-Yang, C. F., Chang, C. C., Liu, W. T., Wang, C. H., and  
994 Wang, J. L.: Analysis of high-ozone episodes using a chemical metric based on the reactivities of organic  
995 precursors, *Journal of Geophysical Research: Atmospheres*, 130, e2025JD043921,  
996 <https://doi.org/10.1029/2025JD043921>, 2025.

997 Paatero, P.: Least squares formulation of robust non-negative factor analysis, *Chemometrics Intelligent  
998 Laboratory Systems*, 37, 23-35, [https://doi.org/10.1016/S0169-7439\(96\)00044-5](https://doi.org/10.1016/S0169-7439(96)00044-5), 1997.

999 Paatero, P. and Tapper, U.: Positive matrix factorization: A non-negative factor model with optimal  
1000 utilization of error estimates of data values, *Environmetrics*, 5, 111-126,  
1001 <https://doi.org/10.1002/env.3170050203>, 1994.

1002 Pallavi, S. B. and Sinha, V.: Source apportionment of volatile organic compounds in the northwest Indo-  
1003 Gangetic Plain using a positive matrix factorization model, *Atmospheric Chemistry and Physics*, 19,  
1004 15467-15482, <https://doi.org/10.5194/acp-19-15467-2019>, 2019.

1005 Park, C., Schade, G. W., and Boedeker, I.: Characteristics of the flux of isoprene and its oxidation  
1006 products in an urban area, *Journal of Geophysical Research: Atmospheres*, 116,  
1007 <https://doi.org/10.1029/2011JD015856>, 2011.

1008 Pedrozo, H. A., Reartes, S. B. R., Diaz, M. S., Vecchiotti, A., and Grossmann, I. E.: Coproduction of  
1009 ethylene and propylene based on ethane and propane feedstocks, in: *Computer Aided Chemical  
1010 Engineering*, Elsevier, 907-912, <https://doi.org/10.1016/B978-0-12-823377-1.50152-X>, 2020.

1011 Pekney, N. J., Davidson, C. I., Zhou, L., and Hopke, P. K.: Application of PSCF and CPF to PMF-  
1012 modeled sources of PM<sub>2.5</sub> in Pittsburgh, *Aerosol Science Technology*, 40, 952-961,  
1013 <https://doi.org/10.1080/02786820500543324>, 2006.

1014 Peron, A., Graus, M., Striednig, M., Lamprecht, C., Wohlfahrt, G., and Karl, T.: Deciphering  
1015 anthropogenic and biogenic contributions to selected non-methane volatile organic compound emissions  
1016 in an urban area, *Atmospheric Chemistry Physics*, 24, 7063-7083, 2024.

1017 Pollack, I., Ryerson, T., Trainer, M., Parrish, D., Andrews, A., Atlas, E. L., Blake, D., Brown, S.,  
1018 Commane, R., and Daube, B.: Airborne and ground-based observations of a weekend effect in ozone,  
1019 precursors, and oxidation products in the California South Coast Air Basin, *Journal of Geophysical  
1020 Research: Atmospheres*, 117, <https://doi.org/10.1029/2011JD016772>, 2012.

1021 Ramírez, A. S., Ramondt, S., Van Bogart, K., and Perez-Zuniga, R.: Public awareness of air pollution

1022 and health threats: challenges and opportunities for communication strategies to improve environmental  
1023 health literacy, *Journal of Health Communication*, 24, 75-83,  
1024 <https://doi.org/10.1080/10810730.2019.1574320>, 2019.

1025 Ren, J. and Xie, S.: Diagnosing ozone-NO<sub>x</sub>-VOC sensitivity and revealing causes of ozone increases in  
1026 China based on 2013–2021 satellite retrievals, *Atmospheric Chemistry Physics Discussions*, 2022, 1-22,  
1027 <https://doi.org/10.5194/acp-22-15035-2022>, 2022.

1028 Rubin, J. I., Kean, A. J., Harley, R. A., Millet, D. B., and Goldstein, A. H.: Temperature dependence of  
1029 volatile organic compound evaporative emissions from motor vehicles, *Journal of Geophysical Research:*  
1030 *Atmospheres*, 111, <https://doi.org/10.1029/2005JD006458>, 2006.

1031 Scheff, P. A., Wadden, R. A., Bates, B. A., and Aronian, P. F.: Source fingerprints for receptor modeling  
1032 of volatile organics, *Japca*, 39, 469-478, <https://doi.org/10.1080/08940630.1989.10466546>, 1989.

1033 Shao, P., An, J., Xin, J., Wu, F., Wang, J., Ji, D., and Wang, Y.: Source apportionment of VOCs and the  
1034 contribution to photochemical ozone formation during summer in the typical industrial area in the  
1035 Yangtze River Delta, China, *Atmospheric Research*, 176, 64-74,  
1036 <https://doi.org/10.1016/j.atmosres.2016.02.015>, 2016.

1037 Shen, L., Xiang, P., Liang, S., Chen, W., Wang, M., Lu, S., and Wang, Z.: Sources profiles of volatile  
1038 organic compounds (VOCs) measured in a typical industrial process in Wuhan, Central China,  
1039 *Atmosphere*, 9, 297, <https://doi.org/10.3390/atmos9080297>, 2018.

1040 Sillman, S.: The relation between ozone, NO<sub>x</sub> and hydrocarbons in urban and polluted rural  
1041 environments, *Atmospheric Environment*, 33, 1821-1845, [https://doi.org/10.1016/S1352-](https://doi.org/10.1016/S1352-2310(98)00345-8)  
1042 [2310\(98\)00345-8](https://doi.org/10.1016/S1352-2310(98)00345-8), 1999.

1043 Song, M., Tan, Q., Feng, M., Qu, Y., Liu, X., An, J., and Zhang, Y.: Source apportionment and secondary  
1044 transformation of atmospheric nonmethane hydrocarbons in Chengdu, Southwest China, *Journal of*  
1045 *Geophysical Research: Atmospheres*, 123, 9741-9763, <https://doi.org/10.1029/2018JD028479>, 2018.

1046 Song, M., Li, X., Yang, S., Yu, X., Zhou, S., Yang, Y., Chen, S., Dong, H., Liao, K., and Chen, Q.:  
1047 Spatiotemporal variation, sources, and secondary transformation potential of VOCs in Xi'an, China,  
1048 *Atmospheric Chemistry Physics Discussions*, 2020, 1-34, <https://doi.org/10.5194/acp-21-4939-2021>,  
1049 2020.

1050 Su, Y.-C., Chen, S.-P., Tong, Y.-H., Fan, C.-L., Chen, W.-H., Wang, J.-L., and Chang, J. S.: Assessment  
1051 of regional influence from a petrochemical complex by modeling and fingerprint analysis of volatile  
1052 organic compounds (VOCs), *Atmospheric Environment*, 141, 394-407,  
1053 <https://doi.org/10.1016/j.atmosenv.2016.07.006>, 2016.

1054 Su, Y. C., Chen, W. H., Fan, C. L., Tong, Y. H., Weng, T. H., Chen, S. P., Kuo, C. P., Wang, J. L., and  
1055 Chang, J. S.: Source Apportionment of Volatile Organic Compounds (VOCs) by Positive Matrix  
1056 Factorization (PMF) supported by Model Simulation and Source Markers - Using Petrochemical  
1057 Emissions as a Showcase, *Environmental Pollution*, 254, 112848,  
1058 <https://doi.org/10.1016/j.envpol.2019.07.016>, 2019.

1059 Swarthout, R. F., Russo, R. S., Zhou, Y., Hart, A. H., and Sive, B. C.: Volatile organic compound

1060 distributions during the NACHTT campaign at the Boulder Atmospheric Observatory: Influence of urban  
1061 and natural gas sources, *Journal of Geophysical Research: Atmospheres*, 118, 10,614-610,637, 2013.

1062 Thiruvenkataswamy, P., Eljack, F. T., Roy, N., Mannan, M. S., and El-Halwagi, M. M.: Safety and techno-  
1063 economic analysis of ethylene technologies, *Journal of Loss Prevention in the Process Industries*, 39, 74-  
1064 84, <https://doi.org/10.1016/j.jlp.2015.11.019>, 2016.

1065 Thompson, C. R., Hueber, J., and Helmig, D.: Influence of oil and gas emissions on ambient atmospheric  
1066 non-methane hydrocarbons in residential areas of Northeastern Colorado, *Elementa*, 3, 000035, 2014.

1067 Vettikkat, L., Miettinen, P., Buchholz, A., Rantala, P., Yu, H., Schallhart, S., Petäjä, T., Seco, R., Männistö,  
1068 E., and Kulmala, M.: High emission rates and strong temperature response make boreal wetlands a large  
1069 source of isoprene and terpenes, *Atmospheric Chemistry Physics*, 23, 2683-2698, 2023.

1070 Wang, C., Li, X., Miao, X., Li, J., Li, Y., Song, C., Yang, Z., Qi, J., and Jin, T.: Diesel vehicle emissions:  
1071 Dissecting the multi-factorial effect on variations of VOC-component concentrations, *Urban Climate*, 58,  
1072 102157, <https://doi.org/10.1016/j.uclim.2024.102157>, 2024.

1073 Wang, H., Lou, S., Huang, C., Qiao, L., Tang, X., Chen, C., Zeng, L., Wang, Q., Zhou, M., and Lu, S.:  
1074 Source profiles of volatile organic compounds from biomass burning in Yangtze River Delta, China,  
1075 *Aerosol Air Quality Research*, 14, 818-828, 2014.

1076 Wang, Q., Li, S., Dong, M., Li, W., Gao, X., Ye, R., and Zhang, D.: VOCs emission characteristics and  
1077 priority control analysis based on VOCs emission inventories and ozone formation potentials in  
1078 Zhoushan, *Atmospheric Environment*, 182, 234-241, <https://doi.org/10.1016/j.atmosenv.2018.03.034>,  
1079 2018.

1080 Wang, W., van der A, R., Ding, J., van Weele, M., and Cheng, T.: Spatial and temporal changes of the  
1081 ozone sensitivity in China based on satellite and ground-based observations, *Atmospheric Chemistry  
1082 Physics*, 21, 7253-7269, <https://doi.org/10.5194/acp-21-7253-2021>, 2021.

1083 Wei, W., Lv, Z., Yang, G., Cheng, S., Li, Y., and Wang, L.: VOCs emission rate estimate for complicated  
1084 industrial area source using an inverse-dispersion calculation method: A case study on a petroleum  
1085 refinery in Northern China, *Environmental Pollution*, 218, 681-688,  
1086 <https://doi.org/10.1016/j.envpol.2016.07.062>, 2016.

1087 Wernis, R. A., Kreisberg, N. M., Weber, R. J., Drozd, G. T., and Goldstein, A. H.: Source apportionment  
1088 of VOCs, IVOCs and SVOCs by positive matrix factorization in suburban Livermore, California,  
1089 *Atmospheric Chemistry and Physics*, 22, 14987-15019, <https://doi.org/10.5194/acp-22-14987-2022>,  
1090 2022.

1091 Wu, F., Yu, Y., Sun, J., Zhang, J., Wang, J., Tang, G., and Wang, Y.: Characteristics, source apportionment  
1092 and reactivity of ambient volatile organic compounds at Dinghu Mountain in Guangdong Province,  
1093 China, *Science of the Total Environment*, 548, 347-359, <https://doi.org/10.1016/j.scitotenv.2015.11.069>,  
1094 2016.

1095 Wu, S., Alaimo, C. P., Green, P. G., Young, T. M., Zhao, Y., Liu, S., Kuwayama, T., and Kleeman, M. J.:  
1096 Source apportionment of Volatile Organic Compounds (VOCs) in the South Coast Air Basin (SoCAB)  
1097 During RECAP-CA, *Atmospheric Environment*, 338, 120847,

1098 <https://doi.org/10.1016/j.atmosenv.2024.120847>, 2024.

1099 Xie, Y. and Berkowitz, C. M.: The use of positive matrix factorization with conditional probability  
1100 functions in air quality studies: an application to hydrocarbon emissions in Houston, Texas, *Atmospheric*  
1101 *Environment*, 40, 3070-3091, <https://doi.org/10.1016/j.atmosenv.2005.12.065>, 2006.

1102 Xu, H., Jia, Y., Sun, Z., Su, J., Liu, Q. S., Zhou, Q., and Jiang, G.: Environmental pollution, a hidden  
1103 culprit for health issues, *Eco-Environment Health*, 1, 31-45, <https://doi.org/10.1016/j.eehl.2022.04.003>,  
1104 2022.

1105 Xu, Z., Huang, X., Nie, W., Chi, X., Xu, Z., Zheng, L., Sun, P., and Ding, A.: Influence of synoptic  
1106 condition and holiday effects on VOCs and ozone production in the Yangtze River Delta region, China,  
1107 *Atmospheric Environment*, 168, 112-124, <https://doi.org/10.1016/j.atmosenv.2017.08.035>, 2017.

1108 Yang, Y., Liu, B., Hua, J., Yang, T., Dai, Q., Wu, J., Feng, Y., and Hopke, P. K.: Global review of source  
1109 apportionment of volatile organic compounds based on highly time-resolved data from 2015 to 2021,  
1110 *Environ Int*, 165, 107330, <https://doi.org/10.1016/j.envint.2022.107330>, 2022.

1111 Yeh, C.-K., Lin, C., Shen, H.-C., Cheruiyot, N. K., Nguyen, D.-H., and Chang, C.-C.: Real-time energy  
1112 consumption and air pollution emission during the transpacific crossing of a container ship, *Scientific*  
1113 *Reports*, 12, 15272, <https://doi.org/10.1038/s41598-022-19605-7>, 2022.

1114 Zeng, J., Zhang, Y., Mu, Z., Pang, W., Zhang, H., Wu, Z., Song, W., and Wang, X.: Temperature and light  
1115 dependency of isoprene and monoterpene emissions from tropical and subtropical trees: Field  
1116 observations in south China, *Applied Geochemistry*, 155, 105727, 2023.

1117 Zhang, K., Li, L., Huang, L., Wang, Y., Huo, J., Duan, Y., Wang, Y., and Fu, Q.: The impact of volatile  
1118 organic compounds on ozone formation in the suburban area of Shanghai, *Atmospheric Environment*,  
1119 232, 117511, <https://doi.org/10.1016/j.atmosenv.2020.117511>, 2020.

1120 Zhang, X., Han, L., Wei, H., Tan, X., Zhou, W., Li, W., and Qian, Y.: Linking urbanization and air quality  
1121 together: A review and a perspective on the future sustainable urban development, *Journal of Cleaner*  
1122 *Production*, 346, 130988, <https://doi.org/10.1016/j.jclepro.2022.130988>, 2022.

1123 Zhang, Y., Li, R., Fu, H., Zhou, D., and Chen, J.: Observation and analysis of atmospheric volatile organic  
1124 compounds in a typical petrochemical area in Yangtze River Delta, China, *Journal of Environmental*  
1125 *Sciences*, 71, 233-248, <https://doi.org/10.1016/j.jes.2018.05.027>, 2018.

1126 Zhang, Y., Wang, X., Zhang, Z., Lü, S., Huang, Z., and Li, L.: Sources of C<sub>2</sub>-C<sub>4</sub> alkenes, the most  
1127 important ozone nonmethane hydrocarbon precursors in the Pearl River Delta region, *Science of the Total*  
1128 *Environment*, 502, 236-245, <https://doi.org/10.1016/j.scitotenv.2014.09.024>, 2015.

1129 Zhou, S., Davy, P. K., Huang, M., Duan, J., Wang, X., Fan, Q., Chang, M., Liu, Y., Chen, W., and Xie,  
1130 S.: High-resolution sampling and analysis of ambient particulate matter in the Pearl River Delta region  
1131 of southern China: source apportionment and health risk implications, *Atmospheric Chemistry and*  
1132 *Physics*, 18, 2049-2064, <https://doi.org/10.5194/acp-18-2049-2018>, 2018.

1133 Zou, Y., Deng, X. J., Deng, T., Yin, C. Q., and Li, F.: One-year characterization and reactivity of isoprene  
1134 and its impact on surface ozone formation at a suburban site in Guangzhou, China, *Atmosphere*, 10, 201,  
1135 <https://doi.org/10.3390/atmos10040201>, 2019.

1136 Zou, Y., Deng, X., Zhu, D., Gong, D., Wang, H., Li, F., Tan, H., Deng, T., Mai, B., and Liu, X.:  
1137 Characteristics of 1 year of observational data of VOCs, NO<sub>x</sub> and O<sub>3</sub> at a suburban site in Guangzhou,  
1138 China, Atmospheric Chemistry and Physics, 15, 6625-6636, <https://doi.org/10.5194/acp-15-6625-2015>,  
1139 2015.  
1140